https://doi.org/10.1016/j.ymssp.2021.108159

High-efficient decoupling method for coupling systems with multiple subdomains and time steps

Peng YUAN and You DONG

Department of Civil and Environmental Engineering, The Hong Kong Polytechnic University, Hong Kong 999077, China

Abstract: This paper proposes a high-efficient decoupling method with energy conservative property for solving a system with multiple subdomains and time steps efficiently. The proposed method can incorporate New General-α integration schemes with desirable algorithmic damping and accuracy to filter spurious high-frequency vibration contents and retain the second-order accuracy. The method can decompose the coupling system into several independent subdomains with different time steps. Different integration schemes can be adopted to solve each subdomain independently. Accuracy and stability for each decoupling subdomain are ensured by adjusting its integration parameters. Desirable algorithmic damping is employed to filter the high-frequency spurious vibration contents by using General-α integration schemes, simultaneously, the second-order accuracy is ensured in solved numerical results. Since vibrations are not split into link vibrations and free vibrations for all decoupling subdomains, computational efficiency is improved significantly compared with existing methods. To derive the decoupling method conveniently, the coupling dynamic system with two subdomains and different time steps is built in a Newmark compact form firstly. Subsequently, a decoupling strategy is formulated to decompose and solve the coupling system independently. Accordingly, New General-α schemes are investigated and incorporated in the proposed method to obtain desirable algorithmic damping and accuracy in numerical results. Finally, three illustrative examples are employed to demonstrate the accuracy, efficiency, energy property, and adaptability for multi-subdomains (≥3) of the proposed method.

Keywords: Decoupling method, Efficiency, Multi-subdomains, Desirable algorithmic damping, Energy conservation, Accuracy.

1 Introduction

Nowadays, as the scale and complexity of engineering problems are increasing significantly, studies are needed to develop more accurate and efficient methods to meet the relevant needs for these complex engineering problems (e.g., safety-related impact simulations for aircraft components, large-scale engineering problems with millions of elements, multi-physical phenomena as coupled fluid-structure problems [1][2]). Considering accuracy, stability, and computational efficiency [3][4][5], a single method (explicit or implicit) is inefficient to solve the above problems by using an entire model with a unique time step. One potential solution is to divide the entire domain into several subdomains. According to the frequency contents, applied loads, and possible nonlinear behaviors of each subdomain [6][7][8], different time steps and schemes (explicit or implicit) can be adopted for different subdomains [9]. Each subdomain is solved independently and efficiently, then coupled with each other [10] at interconnected system time steps.

In recent decades, three classical methods were proposed [2][14] to implement a couple of different subdomains: mixed-method, multi-time-step method, and mixed-multi-time-step method. Mixed method (explicit or implicit) [15]-[23] with a unique time step was proposed by using nodal partitioning or element partitioning [11][12][13]. Multi-time-step method (also called sub-cycling) [24] was proposed and improved [27]-[32]. This algorithm uses nodal groups or element groups to partition the mesh into multiple subdomains that are updated with different time steps [25] [26]. However, proof of stability is available only for some particular time integration schemes with limitation on the time step ratio [33][37], or only statistically stable [34], or with possible numerical dissipation at the interface between different

subdomains [35][36][38][39]. Mixed-multi-time-step method (MMTS) was proposed until the method of finite element tearing and interconnecting (FETI) was developed by Farhat and Roux [40][41][42]. Using FETI method, a complex or large-scale structure can be divided into different subdomains with non-overlapping elements [11][12][13], and each subdomain is solved separately. By imposing velocity continuity conditions on the interfaces shared nodes, Gravouil and Combescure (GC method) proposed [43][44] and improved [49]-[55] the MMTS methods to couple arbitrary Newmark scheme. However, energy conservative can only be retained for the case with a unique time step for all subdomains [1][45]-[48][56]. To address this issue, Prakash and Hjelmstad [9] proposed an algorithm (the PH method) with energy conservative property. Recently, two new coupling methods, BGC-micro and BGC-macro, were developed [2][10] to couple the Newmark scheme and HHT-α scheme in linear dynamics. The BGC-micro and BGC-macro methods with Newmark scheme exactly match GC [43][44] and PH [9], respectively [57]. However, for all MMTS methods, the border program [57] with complex storage should be introduced to solve the coupling dynamic system. More specifically, the dynamic responses of each subdomain are divided into two independent vibrations [58] [59] in the analysis, i.e., vibrations under external loads and vibrations with link forces. Therefore, efficiency of multi-time step coupling methods could be further improved. Furthermore, dynamic equations are built at each micro time step, thus, even though, BGC-Micro/GC is energy dissipative, they are still very promising owing to their ease of implementation compared with BGC_Macro/PH [2]. A potential method combining advantages of the two above methods (GC and PH), i.e., dynamic equations are built at micro time steps and energy conservation is ensured in numerical results, is developed herein.

In this paper, a decoupling method with energy conservative property is proposed for solving a coupling system with multiple subdomains and time steps efficiently. New General-α integration schemes with desirable algorithmic dissipation and accuracy are investigated and incorporated in the method to filter spurious vibration contents and retain the second-order accuracy. The proposed method can decompose the coupling system into several independent subdomains with different time steps. Different integration schemes are then employed to solve each subdomain independently. Accuracy and stability for each independent subdomain can be ensured by adjusting its integration parameters. Desirable algorithmic damping and accuracy can be obtained simultaneously. Computational efficiency is improved significantly.

To illustrate the derivation and demonstration process of the proposed method, the remainder of this paper is organized as follows: Firstly, the compact form of Newmark method is introduced to build the coupling system with multiple subdomains and time steps conveniently. Subsequently, a decoupling strategy is formulated to solve each subdomain independently and efficiently. Accordingly, the decoupling method is implemented, and its energy conservation property is verified. Then, New General-α integration schemes are investigated and incorporated in the proposed method to obtain desirable algorithmic damping and accuracy. Finally, to demonstrate the accuracy, efficiency, energy property, and adaptability for multi-subdomains (≥3), three illustrative examples are investigated.

2 Establishment of coupling system

2.1 Compact form of dynamic equations

A continuous domain Ω, as depicted in Fig. 1 (a), is decomposed into S subdomains by using FETI method [40]. The interconnected subdomains have shared nodes at interfaces Γ_b created

by partitioning of the entire domain Ω. For an individual subdomain, as shown in Fig. 1 (b), additional forces $\boldsymbol{\Lambda}$ are applied to the corresponding subdomains, which leads to interconnect/couple with other subdomains.

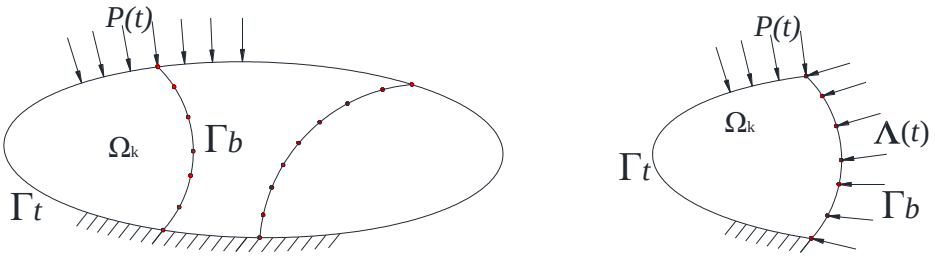

(a) An entire domain (b) a typical subdomain

Fig. 1. A partitioned problem

Hamilton's principle is adopted to build the dynamics equation of the coupling system as follows:

$$\boldsymbol{M}^k\boldsymbol{a}^k + \boldsymbol{C}^k\boldsymbol{v}^k + \boldsymbol{K}^k\boldsymbol{u}^k + \boldsymbol{L}^{k^T}\boldsymbol{\Lambda} = \boldsymbol{P}^k \quad \forall k : 1 \le k \le S \tag{1a}$$

$$\sum_{k=1}^{S} \boldsymbol{L}^k\boldsymbol{v}^k = 0 \tag{1b}$$

where the superscript k on a quantity refers to the corresponding subdomain; $\boldsymbol{M}^k$, $\boldsymbol{K}^k$, $\boldsymbol{C}^k$, $\boldsymbol{P}^k$, $\boldsymbol{u}^k$, and $\boldsymbol{v}^k$ are the mass matrix, stiffness matrix, damping matrix, external excitation vector, displacement vector, and velocity vector of the k^{th} subdomain Ω_k, respectively; $\boldsymbol{\Lambda}$ is a Lagrange multiplier; $\boldsymbol{L}^k$ is a Boolean matrix of dimension $L \times N_k$; and N_k and L are the number of degrees of freedom (DOF) of the k^{th} subdomain Ω_k and its interface Γ_b, respectively. The velocity continuity condition (i.e., Eq. (1b)) is imposed on the interfaces of interconnected subdomains. Further detailed information on Eq. (1) and Boolean matrix can be found in [9][40].

The unknowns in Eq. (1) are the kinematic quantities (i.e., $\boldsymbol{a}^k$, $\boldsymbol{u}^k$, and $\boldsymbol{v}^k$) of all subdomains and Lagrange multipliers $\boldsymbol{\Lambda}$. The multipliers are regarded as interface

reactions/link forces acted on interfaces of interconnected subdomains. In the absence of interface link forces $\boldsymbol{\Lambda}$, all kinematic quantities can be solved by introducing a dynamic method only, e.g., Newmark method or New Generalized-α (NG) [64]. However, for coupled multi-subdomains with different time steps, besides adopting a dynamic method within the solving process, a complementary equation/assumption is also required to solve the intermediated interface link forces at micro time steps (non-system time step)[44]. Simultaneously, zero energy dissipation [45]-[48] needs to be ensured in interfaces of shared nodes.

To conveniently elaborate the computational process for the coupling system with multiple subdomains and time steps, a compact form of the dynamic equation is discussed below firstly. Note that its energy form is only verified strictly [1][11][59] for all dynamic methods with a single time step. Therefore, the compact form of Newmark method is introduced to build and simplify the coupling dynamic equations. To obtain desirable algorithmic damping and accuracy, NG schemes without overshoot are also investigated in the later sections. The expressions of displacement and velocity for Newmark scheme and the incremental form of dynamic equations without damping are, respectively:

$$\boldsymbol{u}_{n+1} = \boldsymbol{u}_n + h\boldsymbol{v}_n + \left(\tfrac{1}{2} - \beta\right)h^2\boldsymbol{a}_n + \beta h^2\boldsymbol{a}_{n+1} \tag{2a}$$

$$\boldsymbol{v}_{n+1} = \boldsymbol{v}_n + h\left((1-\gamma)\boldsymbol{a}_n + \gamma\boldsymbol{a}_{n+1}\right) \tag{2b}$$

$$\boldsymbol{M}\Delta\boldsymbol{a}_{n+1} + \boldsymbol{K}\Delta\boldsymbol{u}_{n+1} + \boldsymbol{L}^T\Delta\boldsymbol{\Lambda}_{n+1} = \Delta\boldsymbol{P}_{n+1} \tag{3}$$

where the subscript is the time step as n indicates time t_n; h is the time step size; and two parameters γ and β are adopted to adjust the accuracy and stability of Newmark scheme. Eq. (2) can be written as the incremental form:

$$\Delta\boldsymbol{u}_{n+1} = \frac{\beta h}{\gamma}\Delta\boldsymbol{v}_{n+1} + h\boldsymbol{v}_n + \frac{\gamma - 2\beta}{2\gamma}h^2\boldsymbol{a}_n \tag{4a}$$

$$\Delta \boldsymbol{a}_{n+1} = \frac{1}{\gamma h}\Delta \boldsymbol{v}_{n+1} - \frac{1}{\gamma}\boldsymbol{a}_n \tag{4b}$$

where Δ is the increment of kinematic quantities from time t_n to t_{n+1}, which are expressed as:

$$\begin{cases} \Delta \boldsymbol{u}_{n+1} = \boldsymbol{u}_{n+1} - \boldsymbol{u}_n \\ \Delta \boldsymbol{v}_{n+1} = \boldsymbol{v}_{n+1} - \boldsymbol{v}_n \\ \Delta \boldsymbol{a}_{n+1} = \boldsymbol{a}_{n+1} - \boldsymbol{a}_n \\ \Delta \boldsymbol{P}_{ext,n+1} = \boldsymbol{P}_{ext,n+1} - \boldsymbol{P}_{ext,n} \\ \Delta \boldsymbol{\Lambda}_{n+1} = \boldsymbol{\Lambda}_{n+1} - \boldsymbol{\Lambda}_n \end{cases} \tag{5}$$

Substituting Eq. (4) into Eq. (3), the dynamic equation is written as:

$$\boldsymbol{K}^* \Delta \boldsymbol{v}_{n+1} + \boldsymbol{L}^T \Delta \boldsymbol{\Lambda}_{n+1} = \boldsymbol{F}_{n+1} \tag{6}$$

where the dynamic operator matrix $\boldsymbol{K}^*$ and the generalized load vector $\boldsymbol{F}_{n+1}$ are, respectively, defined as follows:

$$\boldsymbol{K}^* = \frac{1}{\gamma h}\boldsymbol{M} + \frac{\beta h}{\gamma}\boldsymbol{K} \tag{7}$$

$$\boldsymbol{F}_{n+1} = \Delta \boldsymbol{P}_n - \boldsymbol{K}\left(\frac{\gamma - 2\beta}{2\gamma}h^2 \boldsymbol{a}_n + h\boldsymbol{v}_n\right) + \frac{1}{\gamma}\boldsymbol{M}\boldsymbol{a}_n \tag{8}$$

To simplify the dynamic equations, equations (i.e., Eqs. (4) to (6)) are written in a compact form as follows:

$$\mathbb{K}^* \Delta \mathbb{U}_{n+1} + \mathbb{L}^T \Delta \boldsymbol{\Lambda}_{n+1} = \Delta \mathbb{F}_{n+1} \tag{9}$$

where the generalized load vector is:

$$\Delta \mathbb{F}_{n+1} = \mathbb{P}_{n+1} - \mathbb{N}\mathbb{U}_n \tag{10}$$

The matrices involved in Eqs. (9) and (10) are defined below:

$$\mathbb{K}^* = \begin{bmatrix} \boldsymbol{I} & -\frac{\beta h}{\gamma}\boldsymbol{I} & 0 \\ 0 & \boldsymbol{K}^* & 0 \\ 0 & -\frac{1}{\gamma h}\boldsymbol{I} & \boldsymbol{I} \end{bmatrix} \qquad \mathbb{L}^T = \begin{bmatrix} 0 \\ \boldsymbol{L}^T \\ 0 \end{bmatrix} \tag{11a}$$

$$\mathbb{U}_n=\begin{bmatrix}\boldsymbol{u}_n\\ \boldsymbol{v}_n\\ \boldsymbol{a}_n\end{bmatrix} \qquad \Delta\mathbb{U}_{n+1}=\begin{bmatrix}\Delta\boldsymbol{u}_n\\ \Delta\boldsymbol{v}_n\\ \Delta\boldsymbol{a}_n\end{bmatrix} \tag{11b}$$

$$\mathbb{P}_{n+1}=\begin{bmatrix}0\\ \Delta\boldsymbol{P}_{ext,n}\\ 0\end{bmatrix} \qquad \mathbb{N}=\begin{bmatrix}0 & -h\boldsymbol{I} & -\dfrac{\gamma-2\beta}{2\gamma}h^2\boldsymbol{I}\\ 0 & h\boldsymbol{K} & \dfrac{\gamma-2\beta}{2\gamma}h^2\boldsymbol{K}-\dfrac{1}{\gamma}\boldsymbol{M}\\ 0 & 0 & \dfrac{1}{\gamma}\boldsymbol{I}\end{bmatrix} \tag{11c}$$

To illustrate the coupling process, a domain split into two subdomains with different time steps is discussed below.

2.2 Coupling equations of two subdomains

A domain with two subdomains (A and B) and different time sub-steps (ΔT and Δt), as shown in Fig. 2, is employed to elaborate the coupling method. It is easy to extend to multi-subdomain (≥ 3) system, which is demonstrated in the later sections. The ratio of macro (system) time step ΔT to micro time step Δt is m. The beginning time step and ending time step for the two subdomains are t_0 and t_m, respectively.

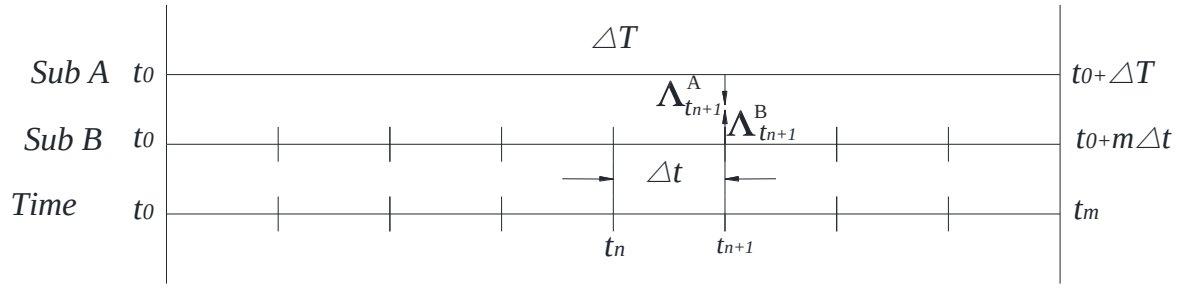

Fig. 2. Two subdomains with different time steps

Dynamic responses of two subdomains are computed by using Eq. (6). More specifically, for subdomain A, dynamic equations built at t_m are:

$$\begin{cases} \boldsymbol{K}_A^* \Delta \boldsymbol{v}_m^A + \boldsymbol{L}_A^T \Delta \boldsymbol{\Lambda}_m^A = \boldsymbol{F}_m^A \\ \Delta \boldsymbol{u}_m^A = \dfrac{\beta_A h_A}{\gamma_A} \Delta \boldsymbol{v}_m^A + h_A \boldsymbol{v}_0^A + \dfrac{\gamma_A - 2\beta_A}{2\gamma_A} h_A^2 \boldsymbol{a}_0^A \\ \Delta \boldsymbol{a}_m^A = \dfrac{1}{\gamma_A h_A} \Delta \boldsymbol{v}_m^A - \dfrac{1}{\gamma_A} \boldsymbol{a}_0^A \end{cases} \tag{12}$$

For subdomain A with macro time steps, a substructure with large-scale, or low-frequency vibrations, or linear behaviors should be assigned to this subdomain to improve computational efficiency. The implicit scheme with unconditional stability for Newmark method is appropriate in this subdomain and the relevant parameters [59][60] are limited as:

$$\gamma \geq 1/2 \; and \; \beta \geq \frac{1}{4}\left(\gamma + \frac{1}{2}\right)^2 \tag{13}$$

Note that when $\gamma = 1/2$, Newmark method is non-dissipation and has second-order accuracy. For $\beta = 1/12$, Newmark method has third-order accuracy [4][5].

For the subdomain B, dynamic equations set at arbitrary time step t_j are:

$$\begin{cases} \boldsymbol{K}_B^* \Delta \boldsymbol{v}_j^B + \boldsymbol{L}_B^T \Delta \Lambda_j^B = \boldsymbol{F}_j^B \\ \Delta \boldsymbol{u}_j^B = \dfrac{\beta_B h_B}{\gamma_B} \Delta \boldsymbol{v}_j^B + h_B \boldsymbol{v}_{j-1}^B + \dfrac{\gamma_B - 2\beta_B}{2\gamma_B} h^2 \boldsymbol{a}_{j-1}^B \\ \Delta \boldsymbol{a}_j^B = \dfrac{1}{\gamma_B h_B} \Delta \boldsymbol{v}_j^B - \dfrac{1}{\gamma_B} \boldsymbol{a}_{j-1}^B \\ \forall j \in \{1, m\} \end{cases} \tag{14}$$

Considering micro time steps, a substructure with small-scale, or high-frequency vibrations, or nonlinear behavior should be assigned in this subdomain to improve accuracy and computational efficiency. Thus, the explicit scheme with the high efficiency and conditional stability is suitable and the relevant parameters [59][60] are limited as:

$$\gamma \geq 1/2 \;\; and \;\; \gamma \geq 2\beta \tag{15}$$

The critical time step size of the explicit scheme [59][60] is:

$$\Delta t \le \frac{1}{\omega_{\max}\sqrt{\gamma/2-\beta}} \tag{16}$$

where ω_{max} is the maximum frequency of a substructure/subdomain. According to structural properties, e.g., frequency content, linearity property, and scale of subdomains, an entire domain can be divided into different subdomains. The implicit and explicit schemes of Newmark method are then used in the corresponding subdomains. The unconditional stability of the implicit schemes and the high efficiency of the explicit schemes are retained in the solving process simultaneously. To efficiently suppress high-frequency spurious vibrations and overshoot and retain the second-order accuracy, simultaneously, New General-α [64][65] (NG) is studied and incorporated to this method in the later sections.

Using the compact form, i.e., Eq. (9), dynamic equations and its continuity condition are, respectively, expressed as follows:

$$\begin{cases} \mathbb{K}_A^* \Delta \mathbb{U}_m^A + \mathbb{L}_A^T \Delta \boldsymbol{\Lambda}_m = \Delta \mathbb{F}_m^A - \mathbb{N}_A \mathbb{U}_0^A \\ \mathbb{K}_B^* \Delta \mathbb{U}_j^B + \mathbb{L}_B^T \Delta \boldsymbol{\Lambda}_j = \Delta \mathbb{F}_j^B - \mathbb{N}_B \mathbb{U}_{j-1}^B \quad \forall j \in \{1, m\} \end{cases} \tag{17}$$

$$\Delta \boldsymbol{v}_A^T \boldsymbol{L}_A^T + \sum_j^m \left(\Delta \boldsymbol{v}_{Bj}^T \boldsymbol{L}_B^T \right) = 0 \tag{18}$$

To solve the above coupling dynamic system, redundant link forces $\boldsymbol{\Lambda}_j$ at intermediated time step t_n need to be assumed/solved firstly. It is worth noting that if link forces are given/solved in the coupling dynamic system, both subdomains can be decoupled into two independent subdomains, information exchange, e.g., displacements, velocities, and accelerations, is only performed at the system time step t_m, and computational efficiency can be improved significantly. Moreover, for the application of multiple subdomains (≥ 3), and the complex and time-consuming recursive coupling approaches [61]-**Error! Reference source not found.** are avoided. Therefore, to solve each subdomain dependently and efficiently, a decoupling strategy

is introduced and demonstrated in the following sections.

3 Decoupling strategy for the coupling system

To decouple the coupling system, supplementary conditions are introduced to solve redundant link forces $\mathbf{\Lambda}_j$ at intermediated time step t_j firstly, which leads to consistency of the number of unknowns and velocity continuity conditions. Subsequently, all subdomains are only coupled at the system time steps (e.g., t_0 and t_m), thus, using the initial information at the beginning time step (i.e., t_0), velocity increments within the system time step are solved for a single subdomain. Additionally, all interface link forces can be solved by substituting the solved velocity increments into the velocity continuity conditions. Finally, using the solved link forces, the coupling system are decomposed into several dependent subdomains, and each subdomain is solved dependently and efficiently. Link force assumption, calculation of velocity increment, and calculation of link forces are discussed successively as below.

3.1 Link force assumption for micro time steps

Responses and link forces of two interconnected subdomains are only coupled at the system time steps, therefore, to calculate intermediated link forces at micro time steps, a linear interpolation is adopted as follows:

$$\mathbf{\Lambda}_j = \left(1-\frac{j}{m}\right)\mathbf{\Lambda}_0 + \frac{j}{m}\mathbf{\Lambda}_m \qquad \forall j \in \{1, m\} \tag{19}$$

where $\mathbf{\Lambda}_0$ and $\mathbf{\Lambda}_m$ refer to the link forces at the beginning (t_0) and end (t_m) system time steps, respectively. According to the assumption, the link force increments are constant as follows:

$$\Delta\mathbf{\Lambda}_j = \Delta\mathbf{\Lambda} \quad \forall j \in \{1, m\} \tag{20}$$

So far, due to the supplementary equation, the number of link forces (i.e., redundant unknown quantities) is identical with the number of the velocity continuity conditions for the coupling dynamic system. Therefore, all link forces can be solved by using corresponding velocity continuity conditions as discussed below.

3.2 Calculation of velocity increment

To solve link forces at the system time step by using velocity continuity conditions, the velocity increment within the system time step ΔT is derived in this section. To calculate the velocity increment within the system time step for an individual subdomain with m time steps, substituting Newmark scheme (Eq. (4)) into the dynamic equation (Eq. (3)), one has:

$$\Delta \boldsymbol{v}_{n+1} = \boldsymbol{K}^{*^{-1}} \left(\Delta \boldsymbol{P}_{n+1} - \boldsymbol{L}^T \Delta \boldsymbol{\Lambda} - \boldsymbol{R}^* \boldsymbol{a}_n - h\boldsymbol{K}\boldsymbol{v}_n \right) \tag{21a}$$

$$\boldsymbol{R}^* = \frac{\gamma - 2\beta}{2\gamma} h^2 \boldsymbol{K} - \frac{1}{\gamma} \boldsymbol{M} \tag{21b}$$

To solve the velocity increment $\Delta \boldsymbol{v}_{n+1}$ at any time step by using the initial system information at time step t_0, e.g., $\boldsymbol{v}_0$, replacing velocity $\boldsymbol{v}_n$ and acceleration $\boldsymbol{a}_n$ items at the right side of Eq. (21a) with $\Delta \boldsymbol{v}_n + \boldsymbol{v}_{n-1}$ and $\Delta \boldsymbol{a}_n + \boldsymbol{a}_{n-1}$ respectively, one has:

$$\Delta \boldsymbol{v}_{n+1} = \boldsymbol{K}^{*^{-1}} \left(\Delta \boldsymbol{P}_{n+1} - \boldsymbol{L}^T \Delta \boldsymbol{\Lambda} - \boldsymbol{R}^* \boldsymbol{a}_{n-1} - h\boldsymbol{K}\boldsymbol{v}_{n-1} - \boldsymbol{R}^* \Delta \boldsymbol{a}_n - h\boldsymbol{K} \Delta \boldsymbol{v}_n \right) \tag{22}$$

Rewriting Eq. (21a) at the time step t_{n-1} and substituting it into the right side of Eq. (22), a recursive expression of velocity increment is derived as follows:

$$\Delta \boldsymbol{v}_{n+1} = \boldsymbol{K}^{*^{-1}} \left(\Delta \boldsymbol{P}_{n+1} - \Delta \boldsymbol{P}_n - \boldsymbol{R}^* \Delta \boldsymbol{a}_n - \left(h\boldsymbol{K} - \boldsymbol{K}^* \right) \Delta \boldsymbol{v}_n \right) \quad (n = 1, 2 \ldots m) \tag{23}$$

Note that the link force item $\Delta \boldsymbol{\Lambda}$ at Eq. (23) has been merged into the velocity and acceleration increments at the time step t_{n-1}. To eliminate the acceleration increment at Eq. (23), the acceleration item at the right of Eq. (4b) is written as:

$$\Delta \boldsymbol{a}_{n+1} = \frac{1}{\gamma h}\Delta \boldsymbol{v}_{n+1} - \frac{1}{\gamma}\left(\Delta \boldsymbol{a}_n + \boldsymbol{a}_{n-1}\right) \tag{24}$$

Rewriting Eq. (4b) at the time step t_n and substituting it into Eq. (24), one has:

$$\Delta \boldsymbol{a}_{n+1} = \frac{1}{\gamma h}\Delta \boldsymbol{v}_{n+1} - \frac{1}{\gamma^2 h}\Delta \boldsymbol{v}_n - \frac{\gamma - 1}{\gamma^2}\boldsymbol{a}_{n-1} \tag{25}$$

Repeating the above procedure, the acceleration increment $\Delta \boldsymbol{a}_{n+1}$ is solved as follows:

$$\Delta \boldsymbol{a}_{n+1} = \frac{1}{\gamma h}\left(\Delta \boldsymbol{v}_{n+1} - \frac{1}{\gamma}\sum_{i=1}^{n}\left(\frac{\gamma - 1}{\gamma}\right)^{i-1}\Delta \boldsymbol{v}_{n+1-i}\right) - \frac{1}{\gamma}\left(\frac{\gamma - 1}{\gamma}\right)^{n}\boldsymbol{a}_0 \quad \left(n = 0,1...m\right) \tag{26}$$

To eliminate the acceleration item at Eq. (23), substituting (26) into Eq. (23), the simplified velocity increment is written as follows:

$$\Delta \boldsymbol{v}_{n+1} = \boldsymbol{K}^{*-1}\begin{pmatrix} \Delta \boldsymbol{P}_{n+1} - \Delta \boldsymbol{P}_n + \frac{1}{\gamma}\left(\frac{\gamma - 1}{\gamma}\right)^{n-1}\boldsymbol{R}^{*}\boldsymbol{a}_0 + \\ \frac{\boldsymbol{R}^{*}}{h\gamma^2}\sum_{i=1}^{n-1}\left(\frac{\gamma - 1}{\gamma}\right)^{i-1}\Delta \boldsymbol{v}_{n-i} - \boldsymbol{GG}\Delta \boldsymbol{v}_n \end{pmatrix} \tag{27a}$$

$$\boldsymbol{GG} = h\left(\beta\frac{1+\gamma}{\gamma^2} - \frac{1+2\gamma}{2\gamma}\right)\boldsymbol{K} + \frac{1+\gamma}{h\gamma^2}\boldsymbol{M} \tag{27b}$$

The velocity increment (Eq. (27)) is a recursive form. Therefore, by substituting the solved velocity increment at the previous steps into Eq. (27) and simplifying them, the velocity increment at arbitrary time step t_{n+1} can be solved by using the first velocity increment $\Delta \boldsymbol{v}_1$ and initial acceleration $\boldsymbol{a}_0$ as follows:

$$\Delta \boldsymbol{v}_{n+1} = \sum_{i=1}^{n-1}\boldsymbol{A}_i\left(\Delta \boldsymbol{P}_{n+2-i} - \Delta \boldsymbol{P}_{n+1-i} + \frac{1}{\gamma}\left(\frac{\gamma - 1}{\gamma}\right)^{n-i}\boldsymbol{R}^{*}\boldsymbol{a}_0\right) + \boldsymbol{A}_{n+1}\boldsymbol{K}^{*}\Delta \boldsymbol{v}_1 \tag{28}$$

where coefficients are defined as:

$$\boldsymbol{A}_{i+1} = \boldsymbol{A}_1\left(\boldsymbol{GG}\,\boldsymbol{A}_i + \frac{1}{h\gamma^2}\boldsymbol{R}^{*}\sum_{k=1}^{i-1}\left(\frac{\gamma - 1}{\gamma}\right)^{i-1-k}\boldsymbol{A}_k\right) \quad \left(i = 1...m-1\right) \tag{29a}$$

$$\boldsymbol{A}_1 = \boldsymbol{K}^{*-1} \tag{29b}$$

The link forces $\Delta\boldsymbol{\Lambda}$ are only involved in the first velocity increment $\Delta \boldsymbol{v}_1$. By adding up all

velocity increments, the total velocity increment over the time interval from t_0 to t_m is solved as:

$$\Delta \boldsymbol{V} = \sum_{j=1}^{m-1} \left(\left(\sum_{i=1}^{j} \boldsymbol{A}_i \right) \left(\Delta \boldsymbol{P}_{m+1-j} - \Delta \boldsymbol{P}_{m-j} + \frac{1}{\gamma} \left(\frac{\gamma - 1}{\gamma} \right)^{m-1-j} \boldsymbol{R}^* \boldsymbol{a}_0 \right) \right) + \left(\sum_{i=1}^{m} \boldsymbol{A}_i \right) \boldsymbol{K}^* \Delta \boldsymbol{v}_1 \tag{30}$$

Simplifying coefficients of Eq. (30), the total velocity increment is rewritten as:

$$\Delta \boldsymbol{V} = \sum_{j=1}^{m-1} \boldsymbol{b}_{m+1-j} \boldsymbol{F}_j + \boldsymbol{b}_1 \boldsymbol{K}^* \Delta \boldsymbol{v}_1 \tag{31a}$$

$$\boldsymbol{b}_i = \sum_{k=1}^{m+1-i} \boldsymbol{A}_k \qquad (i = 1,,,m) \tag{31b}$$

$$\boldsymbol{F}_j = \left(\Delta \boldsymbol{P}_{m+1-j} - \Delta \boldsymbol{P}_{m-j} + \frac{1}{\gamma} \left(\frac{\gamma - 1}{\gamma} \right)^{m-1-j} \boldsymbol{R}^* \boldsymbol{a}_0 \right) \qquad (j = 1,,,m-1) \tag{31c}$$

To solve the link force, the velocity increment $\Delta \boldsymbol{v}_1$ is divided into two parts, i.e., the velocity increment $\Delta \bar{\boldsymbol{v}}_1$ generated by free vibration and the velocity increment $\Delta \boldsymbol{w}_1$ generated by link vibration, as follows:

$$\Delta \boldsymbol{v}_1 = \Delta \bar{\boldsymbol{v}}_1 + \Delta \boldsymbol{w}_1 \tag{32a}$$

$$\Delta \bar{\boldsymbol{v}}_1 = \boldsymbol{K}^{*-1} \left(\Delta \boldsymbol{P}_1 - \boldsymbol{R}^* \boldsymbol{a}_0 - h \boldsymbol{K} \boldsymbol{v}_0 \right) \tag{32b}$$

$$\Delta \boldsymbol{w}_1 = -\boldsymbol{K}^{*-1} \boldsymbol{L}^T \Delta \boldsymbol{\Lambda} \tag{32c}$$

By substituting Eq. (32) into Eq. (31), the total incremental velocity is divided into two parts, i.e., $\Delta \bar{\boldsymbol{V}}$ and $\Delta \boldsymbol{W}$, which are, respectively, written as follows:

$$\Delta \boldsymbol{V} = \Delta \bar{\boldsymbol{V}} + \Delta \boldsymbol{W} \tag{33a}$$

$$\Delta \bar{\boldsymbol{V}} = \sum_{j=1}^{m-1} \boldsymbol{b}_{m+1-j} \boldsymbol{F}_j + \boldsymbol{b}_1 \boldsymbol{K}^* \Delta \bar{\boldsymbol{v}}_1 \tag{33b}$$

$$\Delta \boldsymbol{W} = \boldsymbol{b}_1 \boldsymbol{K}^* \Delta \boldsymbol{w}_1 \tag{33c}$$

3.3 Calculation of link forces

To solve link forces using the interface continuity condition, velocity increment equation of two interconnected subdomains is built at t_m as follows:

$$\boldsymbol{L}_A \Delta \boldsymbol{v}_m^A + \boldsymbol{L}_B \Delta \boldsymbol{V}^B = 0 \tag{34a}$$

$$\Delta \boldsymbol{V}^B = \sum_j^m \left(\Delta \boldsymbol{v}_{Bj}^T \boldsymbol{L}_B^T \right) \tag{34b}$$

Velocity increment of each subdomain is divided into the free vibration and link vibration, the above continuity condition is rewritten as follows:

$$\boldsymbol{L}_A \left(\Delta \bar{\boldsymbol{v}}_m^A + \Delta \boldsymbol{w}_m^A \right) + \boldsymbol{L}_B \left(\Delta \bar{\boldsymbol{V}}^B + \Delta \boldsymbol{W}^B \right) = 0 \tag{35}$$

Considering the constant increment of link forces at micro time steps, i.e., Eq. (20), total link forces are calculated as follows:

$$\Delta \boldsymbol{\Lambda}_m = m \Delta \boldsymbol{\Lambda} \tag{36}$$

The velocity increment under link forces [2][11][14] for the subdomain A is calculated as follows:

$$\Delta \boldsymbol{w}_m^A = -m \boldsymbol{K}_A^{*-1} \boldsymbol{L}_A^T \Delta \boldsymbol{\Lambda} \tag{37}$$

By substituting Eq. (32c) into Eq. (33c), the velocity increment under link forces for the subdomain B is written as follows:

$$\Delta \boldsymbol{W}^B = -\boldsymbol{b}_1 \boldsymbol{L}_B^T \Delta \boldsymbol{\Lambda} \tag{38}$$

According to Eq. (33b), for the subdomain B, the velocity increment under external excitation is:

$$\Delta \bar{\boldsymbol{V}}^B = \boldsymbol{b}_1 \boldsymbol{K}^* \Delta \bar{\boldsymbol{v}}_{\boldsymbol{1}}^B + \sum_{j=1}^{m-1} \boldsymbol{b}_{m+1-j} \boldsymbol{F}_j^B \tag{39}$$

Substituting Eqs. (37) - (39) into the velocity continuity condition, i.e., Eq. (35), one has:

$$\boldsymbol{L}_A\Delta\bar{\boldsymbol{v}}_m^A+\boldsymbol{L}_B\left(\boldsymbol{b}_1\boldsymbol{K}^*\Delta\bar{\boldsymbol{v}}_{\boldsymbol{1}}^B+\sum_{j=1}^{m-1}\boldsymbol{b}_{m+1-j}\boldsymbol{F}_j^B\right)=\left(m\boldsymbol{L}^A\boldsymbol{K}_A^{*\text{-}1}\boldsymbol{L}_A^T+\boldsymbol{b}_1\boldsymbol{L}_B^T\right)\Delta\boldsymbol{\Lambda} \tag{40}$$

The link forces at each micro time step are derived as:

$$\Delta\boldsymbol{\Lambda}=\boldsymbol{H}\setminus\boldsymbol{DV} \tag{41}$$

where $\boldsymbol{H}$ is the condense factor and $\boldsymbol{DV}$ is the velocity quantity related to the two subdomains, which can be written, respectively, as follows.

$$\boldsymbol{H}=m\boldsymbol{L}^A\boldsymbol{K}_A^{*\text{-}1}\boldsymbol{L}_A^T+\boldsymbol{L}^B\boldsymbol{b}_1\boldsymbol{L}_B^T \tag{42a}$$

$$\boldsymbol{DV}=\boldsymbol{L}_A\Delta\bar{\boldsymbol{v}}_m^A+\boldsymbol{L}_B\left(\boldsymbol{b}_1\boldsymbol{K}^*\Delta\bar{\boldsymbol{v}}_{\boldsymbol{1}}^B+\sum_{j=1}^{m-1}\boldsymbol{b}_{m+1-j}\boldsymbol{F}_j^B\right) \tag{42b}$$

So far, all link forces are solved for the coupling system with two subdomains, the coupling system can be decoupled into two independent subdomains. Moreover, it is easy to extend to the case with multi-subdomains (≥ 3) and the detail solving process of link forces is given in Appendix I for a system with three subdomains.

4 Implementation and energy investigation of the proposed method

4.1 Implementation of the decoupling method

The coupling system is decoupled into several dependent subdomains by using solved link forces. Substituting the solved link forces into the coupling equation (17), the coupling system equations are decomposed into two independent equations as follows:

$$\begin{cases}\mathbb{K}_A^*\Delta\mathbb{U}_m^A=\mathbb{R}_m^A-\mathbb{N}_A\mathbb{U}_0^A\\ \mathbb{K}_B^*\Delta\mathbb{U}_j^B=\mathbb{R}_j^B-\mathbb{N}_B\mathbb{U}_{j-1}^B\quad\forall j\in\{1,m\}\end{cases} \tag{43}$$

where the equivalent force matrix $\mathbb{R}_j^B$ is defined below:

$$\mathbb{R}_m^A=\Delta\mathbb{F}_m^A-m\mathbb{L}_B^T\Delta\boldsymbol{\Lambda} \tag{44a}$$

$$\mathbb{R}_j^B=\Delta\mathbb{F}_j^B-\mathbb{L}_B^T\Delta\boldsymbol{\Lambda} \tag{44b}$$

328 Compared with other multi-time-step coupling methods, e.g. the GC method [43][44] and
329 the BGC_Micro method [10][11], loads of all subdomains are not split into external loads and
330 link forces. Corresponding structural vibrations are not divided into free vibration and link
331 vibration. Each subdomain is calculated independently, thus, it is very convenient to extend the
332 method to the application associated with multiple subdomains (≥ 3). Furthermore, complex
333 operations, e.g., determining the number of quantization levels of time steps and the time-step
334 value at each quantization level [62][63], can be avoided by parallel operation of multiple
335 subdomains with different time steps. Therefore, the developed method is featured with
336 decoupling and high-efficiency properties. The flowchart of the solving procedure is given in
337 Appendix II.

338

339 *4.2 Investigation of energy property*

340 The pseudo-energy form of a dynamic system without structure damping is employed to
341 demonstrate the energy property of the proposed method, which is written as:

342 $$\left[\frac{1}{2}\boldsymbol{a}^T\bar{\boldsymbol{A}}\boldsymbol{a}+\frac{1}{2}\boldsymbol{v}^T\boldsymbol{K}\boldsymbol{v}\right]_n^{n+1}=\frac{1}{h}\Delta\boldsymbol{v}^T\Delta\boldsymbol{R}-\left(\gamma-\frac{1}{2}\right)\Delta\boldsymbol{a}^T\bar{\boldsymbol{A}}\Delta\boldsymbol{a} \tag{45a}$$

343 $$\Delta\boldsymbol{R}=\left(\boldsymbol{P}_{n+1}-\boldsymbol{P}_n\right)+\boldsymbol{L}^T\left(\Lambda_{n+1}-\Lambda_n\right) \tag{45b}$$

344 $$\bar{\boldsymbol{A}}=\boldsymbol{M}+\left(\beta-\frac{1}{2}\gamma\right)h^2\boldsymbol{K} \tag{45c}$$

345 Further details on the pseudo-energy are given in [1]. Pseudo-energy form is designated as:

346 $$\Delta E_{kin,n}+\Delta E_{int,n}=\Delta E_{ext,n}+\Delta E_{diss,n} \tag{46a}$$

347 $$\Delta E_{kin,n+1}=\frac{1}{2}\boldsymbol{a}_{n+1}{}^T\bar{\boldsymbol{A}}\boldsymbol{a}_{n+1}-\frac{1}{2}\boldsymbol{a}_n{}^T\bar{\boldsymbol{A}}\boldsymbol{a}_n \tag{46b}$$

$$\Delta E_{\text{int},n+1} = \frac{1}{2}\boldsymbol{v}_{n+1}{}^{T}\boldsymbol{K}\boldsymbol{v}_{n+1} - \frac{1}{2}\boldsymbol{v}_{n}{}^{T}\boldsymbol{K}\boldsymbol{v}_{n} \tag{46c}$$

$$\Delta E_{\text{diss},n+1} = -\left(\gamma - \frac{1}{2}\right)\left[\boldsymbol{a}_{n+1}\right]^{T}\bar{\boldsymbol{B}}\left[\boldsymbol{a}_{n+1}\right] - \left\langle \boldsymbol{a}_{n+1}\right\rangle^{T}\boldsymbol{C}\left\langle \boldsymbol{a}_{n+1}\right\rangle \tag{46d}$$

$$\Delta E_{\text{ext},n+1} = \left[\boldsymbol{v}_{n+1}\right]^{T}\frac{\Delta \boldsymbol{R}}{h} \tag{46e}$$

A subdomain without external loads is employed to discuss the dissipative property, thus, Eq. (46e) is rewritten as:

$$\Delta E_{link,n} = \Delta E_{ext,n} = \frac{1}{h}\Delta \boldsymbol{v}^{T}\left(\boldsymbol{L}^{T}\left(\boldsymbol{\Lambda}_{n+1} - \boldsymbol{\Lambda}_{n}\right)\right) \tag{47}$$

According to the requirements of stability derived in [1] (i.e., $\gamma \geq 1/2$ and $\bar{\boldsymbol{A}}$ are positive definite), the stability of individual subdomain under link forces can be ensured if the first item on the right side of Eq. (45a) is equal to or less than zero. Namely, the pseudo-energy on the left side of Eq. (62), including pseudo kinetic energy $\Delta E_{kin,n}$ and pseudo potential energy $\Delta E_{int,n}$, is bounded and non-divergent.

Similarly, for the domain with two subdomains and different time steps, as shown in Fig. 2, the sum of pseudo-energy is derived as:

$$\begin{aligned}&\Delta E^{A}_{kin,m} + \Delta E^{A}_{\text{int},m} + \sum_{j=1}^{m}\left(\Delta E^{B}_{kin,\text{j}} + \Delta E^{B}_{\text{int,j}}\right) = \\ &\Delta E^{A}_{\text{diss},m} + \sum_{j=1}^{m}\left(\Delta E^{B}_{\text{diss},m}\right) + \Delta E^{A}_{\text{link},m} + \sum_{j=1}^{m}\left(\Delta E^{B}_{\text{link},m}\right)\end{aligned} \tag{48}$$

Referring to Eq. (47), the total interface pseudo-energy for two subdomains with different time steps is written as:

$$\Delta E^{AB}_{\text{link},n} = -\frac{1}{h_A}\Delta \boldsymbol{v}_{A}^{T}\boldsymbol{L}_{A}^{T}\left(\boldsymbol{\Lambda}_{m} - \boldsymbol{\Lambda}_{0}\right) - \sum_{j}^{m}\left(\frac{1}{h_B}\Delta \boldsymbol{v}_{Bj}^{T}\boldsymbol{L}_{B}^{T}\left(\boldsymbol{\Lambda}_{n+1} - \boldsymbol{\Lambda}_{n}\right)\right) \tag{49}$$

Substituting Eq. (19) and the time step ratio (i.e., $h_A = m\,h_B$) into Eq. (49), the total interface

pseudo-energy generated by all link forces is written as follows:

$$\Delta E_{\mathrm{link},n}^{AB} = -\frac{1}{h_B}\left(\Delta \boldsymbol{v}_A^T \boldsymbol{L}_A^T + \sum_j^m \left(\Delta \boldsymbol{v}_{Bj}^T \boldsymbol{L}_B^T \right) \right) \Delta \boldsymbol{\Lambda} \tag{50}$$

Substituting the velocity continuity condition Eq. (18) into Eq. (50), one has:

$$\Delta \boldsymbol{E}_{\mathrm{link},n}^{AB} = 0 \tag{51}$$

Therefore, if the continuity condition (Eq. (18)) and the assumption of linear interpolation of the link forces (Eq. (19)) are fulfilled in the system-solving process, the zero pseudo-energy at the interface of interconnected subdomains can be guaranteed and the entire system is stable. Moreover, the total interface pseudo-energy is only related to link forces, as indicated in Eq. (49), and algorithmic parameters have no influence on the pseudo-energy. It is worth noting that the floating-point operation errors of numerical results could be amplified by the time step h_B and accumulated for pseudo-energy. Therefore, to match the theoretical solution (50), rational number operation should be chosen in the analysis.

5 Extension of New General-α

In the above sections, Newmark method is employed to decouple and solve the coupling system. However, desirable algorithmic damping is often required to filter the spurious high-frequency contents generated by spatial discretization [3][4][5]. Due to desirable accuracy and algorithmic dissipation properties and without overshoot, six integration schemes of NG [64], as given in Table 1, are investigated and incorporated the decoupling system. More information on NG can be obtained in [64]. To decouple the coupling system, link forces are also calculated firstly. More specifically, using the initial information at the beginning system time step (i.e., t_0), velocity increments within the system time step are solved firstly. Subsequently,

substituting the solved velocity increments into the velocity continuity conditions built at time step t_m, all interface link forces are solved. Finally, using the solved link forces, the coupling system are decomposed into several dependent subdomains. Calculations of velocity increment and link forces are discussed successively as below.

Table 1 Algorithmic parameters of NG method

	NOCH-α	CH-α	NOHHT-α	HHT-α	NOWBZ-α	WBZ-α
ρ	[0,1]	[0,1]	[1/2,1]	[1/2,1]	[0,1]	[0,1]
α	$\frac{2\rho-1}{1+\rho}$	$\frac{2\rho-1}{1+\rho}$	0	0	$\frac{\rho-1}{1+\rho}$	$\frac{\rho-1}{1+\rho}$
δ	$\frac{3\rho-1}{2(1+\rho)}$	$\frac{\rho}{1+\rho}$	$\frac{1-\rho}{2(1+\rho)}$	$\frac{1-\rho}{1+\rho}$	$\frac{\rho-1}{2(1+\rho)}$	0
η	$\frac{\rho}{1+\rho}$	$\frac{\rho}{1+\rho}$	$\frac{1-\rho}{1+\rho}$	$\frac{1-\rho}{1+\rho}$	0	0
ε	$\frac{\rho}{(1+\rho)^2}$	$\frac{\rho^2+2\rho-1}{2(1+\rho)^2}$	$\frac{\rho}{(1+\rho)^2}$	$\frac{\rho^2+2\rho-1}{2(1+\rho)^2}$	$\frac{\rho}{(1+\rho)^2}$	$\frac{\rho^2+2\rho-1}{2(1+\rho)^2}$
β	$\frac{1}{(1+\rho)^2}$	$\frac{1}{(1+\rho)^2}$	$\frac{1}{(1+\rho)^2}$	$\frac{1}{(1+\rho)^2}$	$\frac{1}{(1+\rho)^2}$	$\frac{1}{(1+\rho)^2}$
μ	$\frac{\rho}{1+\rho}$	$\frac{3\rho-1}{2(1+\rho)}$	$\frac{\rho}{1+\rho}$	$\frac{3-\rho}{2(1+\rho)}$	$\frac{\rho}{1+\rho}$	$\frac{3\rho-1}{2(1+\rho)}$
γ	$\frac{1}{1+\rho}$	$\frac{3-\rho}{2(1+\rho)}$	$\frac{1}{1+\rho}$	$\frac{3-\rho}{2(1+\rho)}$	$\frac{1}{1+\rho}$	$\frac{3-\rho}{2(1+\rho)}$

Note that ρ is spectral radius and NO- refers to an algorithm without overshoot

5.1 Calculation of velocity increment

The expressions of displacement and velocity and corresponding dynamic equation without damping for NG are, respectively:

$$\begin{aligned}&\boldsymbol{M}\left(\left(1-\alpha\right)\boldsymbol{a}_{n+1}+\alpha\boldsymbol{a}_n\right)+\boldsymbol{K}\left(\left(1-\eta\right)\boldsymbol{u}_{n+1}+\eta\boldsymbol{u}_n\right)\\&=\left(1-\eta\right)\boldsymbol{F}_{n+1}+\eta\boldsymbol{F}_n-\boldsymbol{L}^T\left(\left(1-\eta\right)\boldsymbol{\Lambda}_{n+1}+\eta\boldsymbol{\Lambda}_n\right)\end{aligned} \tag{52}$$

$$\boldsymbol{u}_{n+1}=\boldsymbol{u}_n+h\boldsymbol{v}_n+h^2\left(\varepsilon\boldsymbol{a}_n+\beta\boldsymbol{a}_{n+1}\right) \tag{53a}$$

$$\boldsymbol{v}_{n+1}=\boldsymbol{v}_n+h\left(\mu\boldsymbol{a}_n+\gamma\boldsymbol{a}_{n+1}\right) \tag{53b}$$

Incremental form of NG is written as:

$$\begin{aligned}&\boldsymbol{M}\left(\left(1-\alpha\right)\Delta\boldsymbol{a}_{n+1}+\boldsymbol{a}_{n}\right)+\boldsymbol{K}\left(\left(1-\eta\right)\Delta\boldsymbol{u}_{n+1}+\boldsymbol{u}_{n}\right)\\&=\left(1-\eta\right)\Delta\boldsymbol{F}_{n+1}+\boldsymbol{F}_{n}-\boldsymbol{L}^{T}\left(\left(1-\eta\right)\Delta\boldsymbol{\Lambda}+\boldsymbol{\Lambda}_{n}\right)\end{aligned} \tag{54}$$

$$\Delta\boldsymbol{u}_{n+1}=\frac{\beta h}{\gamma}\Delta\boldsymbol{v}_{n+1}+h\boldsymbol{v}_{n}+\left(\varepsilon-\frac{\beta\mu}{\gamma}\right)h^{2}\boldsymbol{a}_{n} \tag{55a}$$

$$\Delta\boldsymbol{a}_{n+1}=\frac{1}{h\gamma}\Delta\boldsymbol{v}_{n+1}+\left(\frac{\mu}{\gamma}+1\right)\boldsymbol{a}_{n} \tag{55b}$$

where α, δ, η, ε, β, μ, and γ are algorithmic parameters, which are used to adjust accuracy, dissipation, and overshoot. To calculate velocity increment within the system time step for an individual subdomain with m sub-steps, substituting Eq. (55) into Eq. (54), one gets:

$$\bar{\boldsymbol{K}}^{*}\Delta\boldsymbol{v}_{n+1}=\Delta\mathbb{F}_{n+1}-\boldsymbol{L}^{T}\left(\left(1-\eta\right)\Delta\boldsymbol{\Lambda}+\boldsymbol{\Lambda}_{n}\right) \tag{56}$$

where the dynamic operator matrices $\bar{\boldsymbol{K}}^{*}$ and $\bar{\boldsymbol{R}}^{*}$ and the generalized load vector $\Delta\mathbb{F}_{n+1}$ are defined as follows:

$$\Delta\mathbb{F}_{n+1}=\left(1-\eta\right)\Delta\boldsymbol{F}_{n+1}+\boldsymbol{F}_{n}-\left(\boldsymbol{K}\boldsymbol{u}_{n}+\left(1-\eta\right)h\boldsymbol{K}\,\boldsymbol{v}_{n}+\bar{\boldsymbol{R}}^{*}\boldsymbol{a}_{n}\right) \tag{57a}$$

$$\bar{\boldsymbol{K}}^{*}=\left(\frac{\left(1-\alpha\right)}{h\gamma}\boldsymbol{M}+\frac{h\beta\left(1-\eta\right)}{\gamma}\boldsymbol{K}\right) \tag{57b}$$

$$\bar{\boldsymbol{R}}^{*}=\left(\left(1-\eta\right)\frac{\left(\gamma\varepsilon-\beta\mu\right)}{\gamma}h^{2}\boldsymbol{K}+\frac{\left(\alpha\left(\gamma+\mu\right)-\mu\right)}{\gamma}\boldsymbol{M}\right) \tag{57c}$$

The first velocity increment is solved as:

$$\Delta\boldsymbol{v}_{1}=\bar{\boldsymbol{K}}^{*^{-1}}\begin{pmatrix}\left(1-\eta\right)\Delta\boldsymbol{F}_{1}+\boldsymbol{F}_{0}-\boldsymbol{L}^{T}\left(\left(1-\eta\right)\Delta\boldsymbol{\Lambda}+\boldsymbol{\Lambda}_{0}\right)\\-\left(\boldsymbol{K}\boldsymbol{u}_{0}+\left(1-\eta\right)h\boldsymbol{K}\,\boldsymbol{v}_{0}+\bar{\boldsymbol{R}}^{*}\boldsymbol{a}_{0}\right)\end{pmatrix} \tag{58}$$

Using Eq. (55a), displacement recursive function is obtained, which is solved by using initial information of dynamic system as:

$$\Delta \boldsymbol{u}_n = \begin{pmatrix} \left(\frac{-\mu}{\gamma}\right)^{n-1} \frac{\gamma\varepsilon - \beta\mu}{\gamma} h^2 \boldsymbol{a}_0 + h\boldsymbol{v}_0 + \\ \sum_{i=1}^{n-1} \left(1 + \left(\frac{-\mu}{\gamma}\right)^{i-1} \frac{\gamma\varepsilon - \beta\mu}{\gamma^2}\right) h\Delta \boldsymbol{v}_{n-i} + \frac{\beta h}{\gamma} \Delta \boldsymbol{v}_n \end{pmatrix} \tag{59}$$

Using Eq. (55b), acceleration recursive function is derived as follows:

$$\Delta \boldsymbol{a}_{n+1} = \frac{1}{h\gamma}\left(\Delta \boldsymbol{v}_n - \frac{\gamma+\mu}{\gamma}\sum_{i=1}^{n-1}\left(\frac{-\mu}{\gamma}\right)^{i-1} \Delta \boldsymbol{v}_{n-i}\right) - \frac{\gamma+\mu}{\gamma}\left(\frac{-\mu}{\gamma}\right)^{n-1} \boldsymbol{a}_0 \tag{60}$$

Substituting displacement (Eq. (59)) and acceleration (Eq. (60)) into velocity expression (Eq. (56)), velocity recursive function is derived as:

$$\Delta \boldsymbol{v}_{n+1} = \bar{\boldsymbol{K}}^{*-1} \begin{pmatrix} (1-\eta)\boldsymbol{F}_{n+1} + (2\eta - 1)\boldsymbol{F}_n - \eta \boldsymbol{F}_{n-1} \\ -\boldsymbol{L}^T\left((1-\eta)\Delta\boldsymbol{\Lambda} + \boldsymbol{\Lambda}_n\right) \\ -h\boldsymbol{K}\boldsymbol{u}_0 - \left(\frac{-\mu}{\gamma}\right)^{n-1} \boldsymbol{R}\boldsymbol{R}\, \boldsymbol{a}_0 + \boldsymbol{Q}\boldsymbol{Q}\Delta \boldsymbol{v}_n \\ -h\sum_{i=1}^{n-1}\left(\boldsymbol{K} + \frac{1}{\gamma h^2}\left(\frac{-\mu}{\gamma}\right)^{i-1} \boldsymbol{R}\boldsymbol{R}\right)\Delta \boldsymbol{v}_{n-i} \end{pmatrix} \tag{61}$$

where coefficients matrices involved in Eq. (61) are designed as:

$$\boldsymbol{R}\boldsymbol{R} = a1\boldsymbol{K} + a2\boldsymbol{M} \tag{62}$$

$$a1 = h^2 \frac{(\gamma\varepsilon - \beta\mu)(\gamma\eta - (1-\eta)\mu)}{\gamma^2} \tag{63a}$$

$$a2 = \frac{(\gamma+\mu)(\mu - \alpha(\gamma+\mu))}{\gamma^2} \tag{63b}$$

$$\boldsymbol{Q}\boldsymbol{Q} = a3\boldsymbol{M} + a4\boldsymbol{K} \tag{64}$$

$$a3 = \frac{1-2\alpha}{h\gamma} + \frac{(1-\alpha)\mu}{h\gamma^2} \tag{65a}$$

$$a4 = h\left(\eta - 1 - \frac{\varepsilon(1-\eta)+\beta\eta}{\gamma} + \frac{\beta(1-\eta)\mu}{\gamma^2}\right) \tag{65b}$$

Substituting the solved velocity increment at the previous steps into Eq. (61) and simplifying them, by using the first velocity increment $\Delta \boldsymbol{v}_1$ and initial acceleration $\boldsymbol{a}_0$, the velocity increment at arbitrary time step t_{n+1} can be solved as follows:

$$\Delta \boldsymbol{v}_{n+1} = \sum_{i=1}^{n} \bar{\boldsymbol{A}}_i \begin{pmatrix} (1-\eta)\boldsymbol{F}_{n+1} + (2\eta-1)\boldsymbol{F}_n - \eta \boldsymbol{F}_{n-1} \\ -\boldsymbol{L}^T \Delta \boldsymbol{\Lambda} - h\boldsymbol{K}\boldsymbol{u}_0 - \left(\frac{-\mu}{\gamma}\right)^{n-1} \boldsymbol{R}\boldsymbol{R}\,\boldsymbol{a}_0 \end{pmatrix} + \bar{\boldsymbol{K}}^* \bar{\boldsymbol{A}}_{n+1} \boldsymbol{v}_1 \tag{66}$$

where coefficients matrices $\bar{\boldsymbol{A}}_i$ are defined as:

$$\bar{\boldsymbol{A}}_{i+1} = \bar{\boldsymbol{K}}^{*-1} \left(\boldsymbol{Q}\boldsymbol{Q}\bar{\boldsymbol{A}}_i - h\sum_{i=1}^{n-1} \left(\boldsymbol{K} + \left(\frac{-\mu}{\gamma}\right)^{n-1-i} \frac{\boldsymbol{R}\boldsymbol{R}}{\gamma h^2} \right) \bar{\boldsymbol{A}}_i \right) \quad (i = 1 \ldots m-1) \tag{67a}$$

$$\bar{\boldsymbol{A}}_1 = \bar{\boldsymbol{K}}^{*-1} \tag{67b}$$

By adding up each velocity increment and substituting $\Delta \boldsymbol{v}_1$ into the solved sum, the total velocity increment within the system time step can be solved as:

$$\Delta \boldsymbol{V} = \Delta \boldsymbol{V}_1 + \Delta \boldsymbol{V}_2 + \Delta \boldsymbol{V}_3 \tag{68}$$

where velocity increment is divided into three parts as follows:

$$\Delta \boldsymbol{V}_1 = \sum_{j=1}^{m-1} \left(\left(\sum_{i=1}^{j} \bar{\boldsymbol{A}}_i \right) \left((1-\eta)\boldsymbol{F}_{n+1} + (2\eta-1)\boldsymbol{F}_n - \eta \boldsymbol{F}_{n-1} - h\boldsymbol{K}\boldsymbol{v}_0 - \left(\frac{-\mu}{\gamma}\right)^{n-1} \boldsymbol{R}\boldsymbol{R}\,\boldsymbol{a}_0 \right) \right) \tag{69}$$

$$\Delta \boldsymbol{V}_2 = \left(\sum_{i=1}^{m} \boldsymbol{A}_i \right) \left(\eta \boldsymbol{F}_0 + (1-\eta)\boldsymbol{F}_1 - \boldsymbol{K}\left(\boldsymbol{u}_0 + (1-\eta)h\boldsymbol{v}_0\right) - \bar{\boldsymbol{R}}^* \boldsymbol{a}_0 - \boldsymbol{L}^T \boldsymbol{\Lambda}_0 \right) \tag{70}$$

$$\Delta \boldsymbol{V}_3 = \left(\sum_{i=1}^{m} (m+1-i)\bar{\boldsymbol{A}}_i - \eta \sum_{i=1}^{m} \bar{\boldsymbol{A}}_i \right) \boldsymbol{L}^T \Delta \boldsymbol{\Lambda} \tag{71}$$

5.2 Calculation of link forces

For a domain split into two subdomains, the interface continuity condition built at t_m is given

in Eq. (34). The velocity increment of each subdomain is divided into free vibration and link vibration, which is rewritten in Eq. (35). Note that the linear interpolation of the link forces (Eq. (19)) is still assumed in the computational processing. The velocity increments under external forces and link forces for subdomain A are, respectively:

$$\Delta\bar{\boldsymbol{v}}_m^A = \bar{\boldsymbol{K}}_A^{*-1}\Delta\mathbb{F}_{n+1} \tag{72}$$

$$\Delta\boldsymbol{w}_m^A = -\bar{\boldsymbol{K}}_A^{*-1}\boldsymbol{L}_A^T\left(m(1-\eta)\Delta\boldsymbol{\Lambda}+\boldsymbol{\Lambda}_0\right) \tag{73}$$

Velocity increment for the subdomain B can be computed as follows:

$$\Delta\boldsymbol{V}^B = \Delta\boldsymbol{V}_1^B + \Delta\boldsymbol{V}_2^B + \Delta\boldsymbol{V}_3^B \tag{74}$$

$\Delta\boldsymbol{V}_1^B$ $\Delta\boldsymbol{V}_2^B$, and $\Delta\boldsymbol{V}_3^B$ can be solved by using Eq. 69, Eq. 70, and Eq. 71, respectively. Substituting Eqs. (72) - (74) into the velocity continuity condition, i.e., Eq. (35), one has:

$$\begin{aligned}&\boldsymbol{L}_A\bar{\boldsymbol{K}}_A^{*-1}\left(\Delta\mathbb{F}_{n+1}-\boldsymbol{L}_A^T\left(m(1-\eta)\Delta\boldsymbol{\Lambda}+\boldsymbol{\Lambda}_0\right)\right)+\\&\boldsymbol{L}_B\left(\Delta\boldsymbol{V}_1^B+\Delta\boldsymbol{V}_2^B+\left(\sum_{i=1}^{m}(m+1-i)\bar{\boldsymbol{A}}_i^B-\eta\sum_{i=1}^{m}\bar{\boldsymbol{A}}_i^B\right)\boldsymbol{L}_B^T\Delta\boldsymbol{\Lambda}\right)=0\end{aligned} \tag{75}$$

The link force at each micro time step is derived as:

$$\Delta\boldsymbol{\Lambda}_2 = \boldsymbol{H}_2 \setminus \boldsymbol{DV}_2 \tag{76}$$

where $\boldsymbol{H}_2$ is the condense factor and $\boldsymbol{DV}_2$ is the velocity quantity related to the two subdomains, which can be written, respectively, as follows.

$$\boldsymbol{H}_2 = m(1-\eta)\boldsymbol{L}_A\bar{\boldsymbol{K}}_A^{*-1}\boldsymbol{L}_A^T - \boldsymbol{L}_B\left(\sum_{i=1}^{m}(m+1-i)\bar{\boldsymbol{A}}_i^B-\eta\sum_{i=1}^{m}\bar{\boldsymbol{A}}_i^B\right)\boldsymbol{L}_B^T \tag{77a}$$

$$\boldsymbol{DV}_2 = \boldsymbol{L}_A\bar{\boldsymbol{K}}_A^{*-1}\left(\Delta\mathbb{F}_{n+1}-\boldsymbol{L}_A^T\boldsymbol{\Lambda}_0\right)+\boldsymbol{L}_B\left(\Delta\boldsymbol{V}_1^B+\Delta\boldsymbol{V}_2^B\right) \tag{77b}$$

So far, link forces of each subdomain are solved by using NG, the coupling system can be decoupled two independent subdomains, and it is easy to extend to the case with multi-subdomains (≥ 3).

467 *5.3 Implementation for the decoupling method*

468 The entire domain is decoupled into several dependent subdomains by using solved link forces.
469 Substituting the solved link forces (Eq. (76)) into the coupling equations, the decoupling system
470 with different time steps can be solved successively. Using dynamic equation (56), two
471 decoupling equations are written as:

472
$$\begin{cases} \bar{\boldsymbol{K}}_A^* \Delta \boldsymbol{v}_m^A = \mathbb{F}_m^A - \boldsymbol{L}_A^T \left(m\left(1-\eta^A\right)\Delta\boldsymbol{\Lambda} + \boldsymbol{\Lambda}_0 \right) \\ \bar{\boldsymbol{K}}_B^* \Delta \boldsymbol{v}_j^B = \mathbb{F}_j^B - \boldsymbol{L}_B^T \left(\left(1-\eta^B\right)\Delta\boldsymbol{\Lambda} + \boldsymbol{\Lambda}_j \right) \quad \forall j \in \{1, m\} \end{cases} \tag{78}$$

473 where the intermediated link forces $\boldsymbol{\Lambda}_j$, which can be determined by Eq. (19). Desirable
474 algorithmic damping can be employed to filter the high-frequency spurious vibration contents
475 by using NG schemes. Simultaneously, the second-order accuracy is ensured in computed
476 results. It has to highlight that for all dynamic methods with a single time step, the energy form
477 is verified strictly [1][11][59] only for Newmark method. Therefore, for NG schemes,
478 numerical demonstration of energy property is conducted in the following sections.

479

480 **6 Numerical Examples**

481 In this section, three numerical examples are studied to demonstrate decoupling property,
482 energy property, accuracy, and efficiency for the developed seven schemes, including NM
483 (Newmark), CH, HHT, WBZ, NOCH, NOHHT, and NOWBZ. The first example, a single DOF
484 oscillator split into two subdomains, is employed to investigate energy conservative property
485 and accuracy by comparing with existing multi-time-step coupling methods, e.g., PH [9], GC
486 [54], BGC_Macro [11], and BGC_Micro [11].

487 It is not easy to expand the application to multiple subdomains (≥ 3) for other multi-time-

step methods. Thus, to demonstrate the adaptability for multi-subdomains, responses of the oscillator, split into three subdomains, are solved by using the developed method and theoretical solution.

The second example, a wellbore structure decomposed into two independent subdomains, is adopted to investigate the accuracy and computational efficiency of the proposed methods within the application to a system with multi-DOFs.

*6.1 A*n oscillator split into two subdomains

The mass and stiffness of the oscillator, as depicted in Fig 3 (a), are $\bar{m} = 2 \times 10^{-6}$ and $k = 2 \times 10^{4}$, respectively. The equilibrium equation and the initial conditions are:

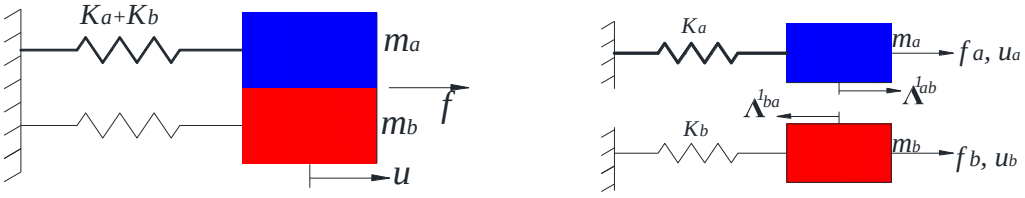

(a) entire oscillator (b) split oscillator

Fig. 3. A split single DOF problem

$$\begin{aligned} a(t) + \omega^2 u(t) &= 0 \\ u(0) = 1, v(0) &= 0 \end{aligned} \tag{79}$$

where $\omega = \sqrt{k / \bar{m}}$ is the angular frequency. The oscillator is split into two single DOF, as shown in Fig. 3 (b), i.e., subdomain A (Sub_A) and subdomain (Sub_B), and mass and stiffness are $M_a = M_b = 1 \times 10^{-6}$ and $K_a = K_b = 1 \times 10^{4}$, respectively. The period and simulation time are $T = 2\pi \times 10^{-5}$ *s* and $\Delta T = 0.01$ *s*, respectively. Considering stability (i.e., Eq. (16)) and accuracy of the integration scheme [5][9], the critical time step h_{crit} is limited to 2×10^{-5} s.

To analyze the energy property, accumulative interface pseudo-energy, and interface mechanical energy [59] are discussed below. Furthermore, to evaluate the accuracy property

under different parameters [5], different cases, e.g., different time step sizes of the two subdomains, various time step ratios m, and different algorithmic parameters β, are investigated.

1) Discussion of interface energy

The interface pseudo-energy given in Eq. (49) and the following classical mechanical energy derived in [59] are assessed for the oscillator.

$$\begin{aligned}&\left[\frac{1}{2}\boldsymbol{v}^T\boldsymbol{M}\boldsymbol{v}+\frac{1}{2}\boldsymbol{u}^T\boldsymbol{K}\boldsymbol{u}+\left(\beta-\frac{1}{2}\gamma\right)\frac{1}{2}h^2\boldsymbol{a}^T\boldsymbol{M}\boldsymbol{a}\right]_n^{n+1}\\&=\Delta\boldsymbol{u}_A^T\left\{\frac{1}{2}\left(\boldsymbol{\Lambda}_{n+1}+\boldsymbol{\Lambda}_n\right)+\left(\gamma-\frac{1}{2}\right)\Delta\boldsymbol{\Lambda}\right\}\\&\quad-\left(\gamma-\frac{1}{2}\right)\left\{\Delta\boldsymbol{u}^T\boldsymbol{K}\Delta\boldsymbol{u}+\left(\beta-\frac{1}{2}\gamma\right)\frac{1}{2}h^2\boldsymbol{a}^T\boldsymbol{M}\boldsymbol{a}\right\}\end{aligned}\tag{80}$$

Each part of the mechanical energy is designated as:

$$\Delta W_{kin,n}+\Delta W_{int,n}+\Delta W_{comp,n}=\Delta W_{ext,n}+\Delta W_{diss,n}\tag{81a}$$

$$\Delta W_{kin,n}=\frac{1}{2}\boldsymbol{v}_{n+1}{}^T\boldsymbol{M}\boldsymbol{v}_{n+1}-\frac{1}{2}\boldsymbol{v}_n{}^T\boldsymbol{M}\boldsymbol{v}_n\tag{81b}$$

$$\Delta W_{int,n}=\frac{1}{2}\boldsymbol{u}_{n+1}{}^T\boldsymbol{K}\boldsymbol{u}_{n+1}-\frac{1}{2}\boldsymbol{u}_n{}^T\boldsymbol{K}\boldsymbol{u}_n\tag{81c}$$

$$\Delta W_{comp,n}=\frac{1}{2}\left(\beta-\frac{1}{2}\gamma\right)h^2\left(\boldsymbol{a}_{n+1}{}^T\boldsymbol{M}\boldsymbol{a}_{n+1}-\boldsymbol{a}_n{}^T\boldsymbol{M}\boldsymbol{a}_n\right)\tag{81d}$$

$$\Delta W_{ext,n}=\Delta\boldsymbol{u}_A^T\left\{\frac{1}{2}\left(\boldsymbol{\Lambda}_{n+1}+\boldsymbol{\Lambda}_n\right)+\left(\gamma-\frac{1}{2}\right)\Delta\boldsymbol{\Lambda}\right\}\tag{81e}$$

$$\Delta W_{ext,n}=-\left(\gamma-\frac{1}{2}\right)\left\{\Delta\boldsymbol{u}^T\boldsymbol{K}\Delta\boldsymbol{u}+\left(\beta-\frac{1}{2}\gamma\right)\frac{1}{2}h^2\boldsymbol{a}^T\boldsymbol{M}\boldsymbol{a}\right\}\tag{81f}$$

More details can be found in [59]. Link forces are served as external excitations for a single subdomain without external excitations. Therefore, the classical interface mechanical energy for a two-subdomain system can be calculated as:

$$\Delta W_{\text{interface},n}^{AB} = -\Delta \boldsymbol{u}_A^T \boldsymbol{L}_A^T \left[\frac{1}{2}\left(\boldsymbol{\Lambda}_m + \boldsymbol{\Lambda}_0\right) + \left(\gamma^A - \frac{1}{2}\right)\Delta\boldsymbol{\Lambda} \right] - \sum_j^m \left\{ \Delta \boldsymbol{v}_{Bj}^T \boldsymbol{L}_B^T \frac{1}{2}\left(\boldsymbol{\Lambda}_j + \boldsymbol{\Lambda}_{j-1}\right) + \left(\gamma^B - \frac{1}{2}\right)\Delta\boldsymbol{\Lambda} \right\} \tag{82}$$

According to Eq. (81a), the interface mechanical energy is equivalent to:

$$\Delta W_{\text{interface},n}^{AB} = \left(\Delta W_{kin,n} + \Delta W_{int,n}\right) - \Delta W_{initial,n} \tag{83}$$

where $\Delta W_{initial,n} = 1 \times 10^4$ is the initial mechanical energy of the oscillator. Furthermore, under the assumption of the linear interpolation of link forces (i.e., Eq. (19)) and the velocity continuity condition (i.e., Eq. (18)), the pseudo-energy (Eq. (51)) is zero for a dynamic system, and algorithmic parameters have no influence on pseudo-energy. The total pseudo-energy at Eq. (51) can be solved as:

$$\Delta E_{\text{link},n}^{AB} = \left(\Delta E_{kin,m}^{A} + \Delta E_{\text{int},m}^{A}\right) + \sum_{j=1}^{m}\left(\Delta E_{kin,\text{j}}^{B} + \Delta E_{\text{int,j}}^{B}\right) = 0 \tag{84}$$

To investigate energy dissipation at interfaces, the accumulative interface mechanical energy and pseudo-energy over a whole calculated time are, respectively:

$$\Delta W_{\text{interface}} = \sum_{i=1}^{T} \Delta W_{\text{interface,i}}^{AB} \tag{85}$$

$$\Delta E_{\text{interface}} = \sum_{i=1}^{T} \Delta E_{\text{interface,i}}^{AB} \tag{86}$$

To eliminate the influence of algorithmic dissipation (i.e., Eq. (46d) and Eq. (81d)) on the interface energy, the accumulative interface mechanical energies without algorithmic dissipation, from 0.0098 *s* to 0.01 *s*, are compared in Fig. 4. Fig. 4 (a) shows that compared with the import initial energy $\Delta W_{initial,n}$, accumulative interface mechanical energies are extremely small and non-attenuated for the coupling methods, e.g. PH, BGC_Macro, and the presented method. Furthermore, according to the parity of time steps, the accumulative

interface mechanical energies are divided into two continuous periodic vibrations without attenuation, as depicted in Fig. 4 (b) and Fig. 4 (c). Therefore, the mechanical energy of the methods above is conservative. It has to highlight that the interface mechanical energy at Eq. (82) and the pseudo-energy at Eq. (49) are derived from Newmark scheme and are not suitable for NG schemes. However, six schemes of NG in Table 1 have the same displacement and velocity integration schemes with Newmark [64] when $\rho = 1$. Therefore, curves of accumulative interface mechanical energy are overlapped for all energy conservation schemes. Fig. 4 (d) shows that even the non-dissipative Newmark scheme ($(\gamma, \beta) = (1/2, 1/4)$) is employed in the coupling methods, the accumulative interface mechanical energy still gradually increases with time for both GC and BGC_Micro, and approaches the initial import mechanical energy at the end time (0.01 s). Therefore, the two methods are energy dissipative in terms of classical mechanical energy.

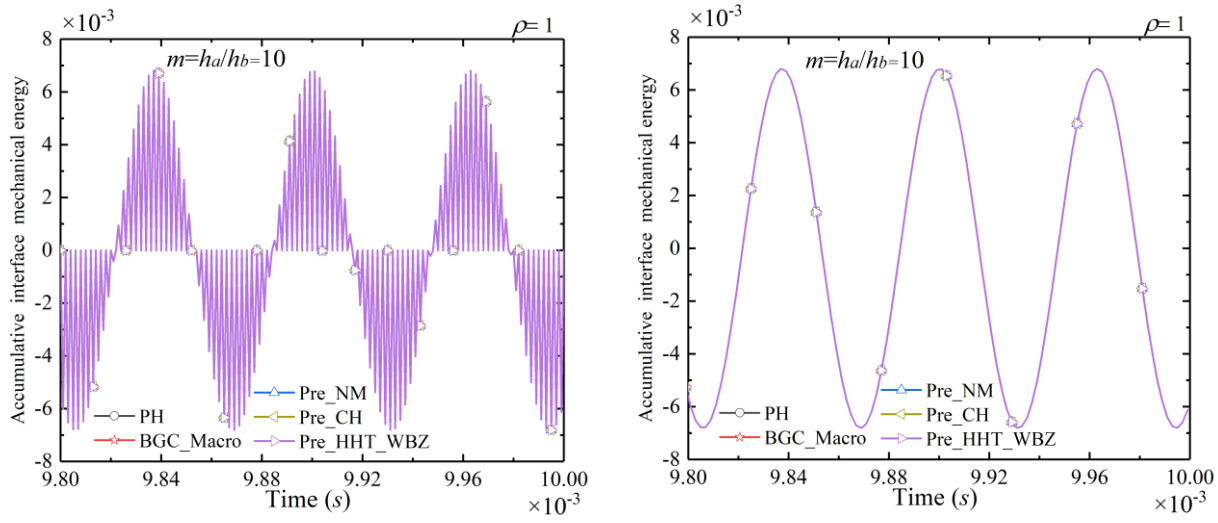

(a) Energy conservative coupling methods (b) Odd time steps

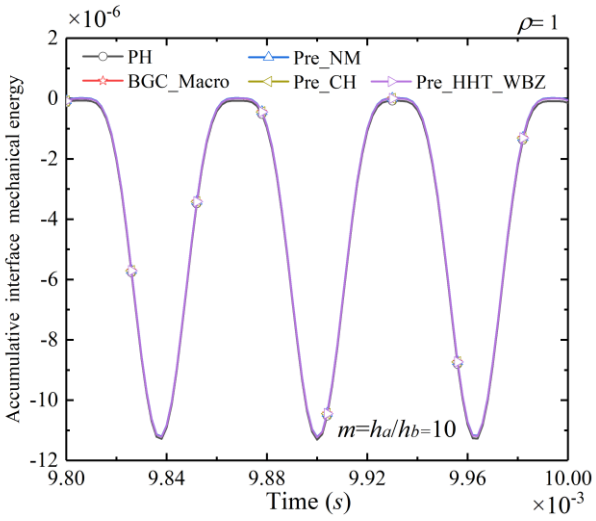

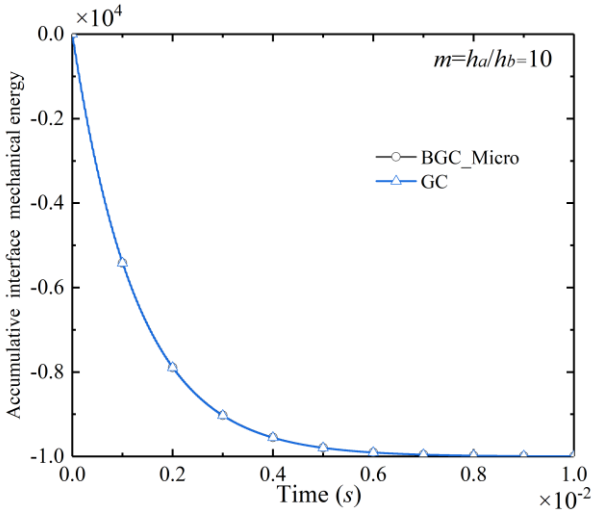

(c) Even time steps (d) Energy dissipative coupling methods

Fig. 4. Accumulative interface mechanical energy of various coupling methods (ρ = 1 and m = 10)

Note that Pre_() denotes the developed method with specified schemes as Pre_NM represents the proposed method with Newmark scheme. The time steps for Sub_A and Sub_B are 1×10^{-6} and 1×10^{-7}, respectively, and the time step ratio is m = 10.

Curves of accumulative interface pseudo-energy are plotted in Fig. 5 for different coupling methods. It shows that for the dissipative coupling methods, e.g. GC and BGC_Micro, the accumulative pseudo-energy gradually dissipates with time and approaches the initial import pseudo-energy $\Delta E_{initial,n} = 1 \times 10^{14}$ at the end time (0.01 s). On the contrary, for the energy conservative coupling methods, pseudo-energy is zero, and the results can also be directly derived from Eq. (51). It is worth noting that the initial pseudo-energy is a large number for the oscillator and the amplitude of pseudo-energy is close to 8.3×10^{10} for both subdomains. To avoid the floating-point operation errors and accurately calculate pseudo-energy, rational number operation should be chosen. Therefore, the proposed methods are featured with the energy conservative property in terms of the interface pseudo-energy.

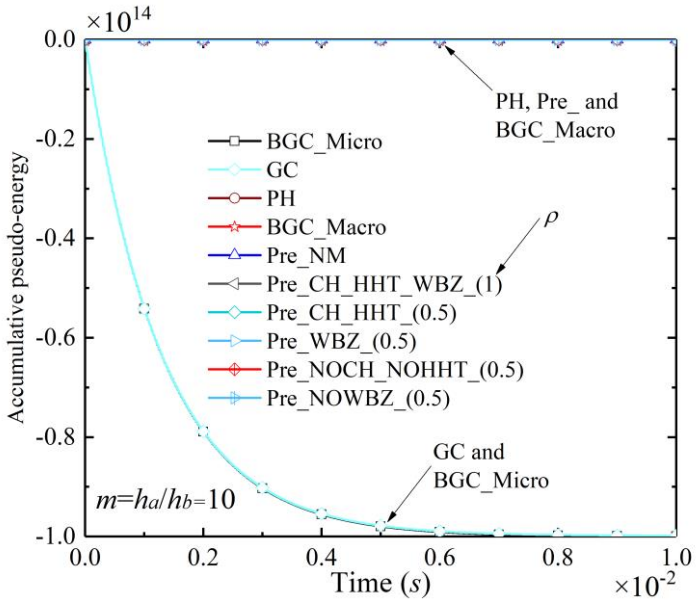

Fig. 5. Pseudo-energy of various coupling methods (m = 10)

Note that the number in brackets following the presented method refers to ρ. NG schemes (ρ = 0.5) are also analogously calculated by using Eq. (86).

2) *Investigation of accuracy*

The absolute error (YP) derived in literature [5] is introduced to investigate accuracy and consistency of the proposed method. The expressions of the YP for Sub_A and Sub_B are, respectively:

$$Err\_a = \sqrt{Ea / E} \tag{87}$$

$$Err\_b = \sqrt{Eb / E} \tag{88}$$

$$Ea = \sum_{i=1}^{N} \left(Wa_{simu}^{i} - W_{theo}^{i} \right)^2 \qquad i = 1,2,,,N \tag{89a}$$

$$Eb = \sum_{i=1}^{N} \left(Wb_{simu}^{m*(i-1)+1} - W_{theo}^{i} \right)^2 \qquad i = 1,2,,,N \tag{89b}$$

$$E = \sum_{i=1}^{N} \left(W_{theo}^{i} \right)^2 \qquad i = 1,2,,,N \tag{89c}$$

where Wa_{simu}^{i}, $Wb_{simu}^{m*(i-1)+1}$, and W_{theo}^{i} are two numerical solutions of Sub_A and Sub_B, and

592 the theoretical solutions, respectively, at the time step t_i. The theoretical solutions are:

593 $$W_{theo}^{i} = u(0)\cos\omega t_i \tag{90}$$

594 To evaluate accuracy under different parameters [5], different time step sizes, various time

595 step ratios m, and different algorithmic parameters β, are investigated below.

596 *Various time step sizes*

597 To analyze accuracy under different time step sizes, error curves, varying with time step

598 sizes, of responses are shown in Fig. 6. Newmark method with (1/2, 1/4) and the macro time

599 step is used to calculate the entire oscillator for the purpose of accuracy comparison. Some

600 findings are observed that absolute errors of computed quantities (including displacements,

601 velocities, and accelerations) increase with the reduced angular frequency (Φ_A [11]) for all

602 coupling integration methods. For energy conservative methods, all quantities of two

603 subdomains have smaller YP than that of Newmark, as marked in Fig. 6. On the contrary, due

604 to energy dissipation at interfaces, the energy dissipative methods, e.g., GC and BGC_Micro,

605 have a larger error than that of Newmark. Moreover, the numerical results of YP show that

606 Sub_B with micro time step (h_A/m) is more accurate than that of Sub_A with macro time step.

607 Thus, the proposed coupling method maintains the second-order accuracy. It is worth noting

608 that all integration schemes have the same displacement and velocity interpolation schemes

609 with Newmark [64] when ρ = 1, thus, the same absolute errors are observed in energy

610 conservative methods and energy dissipative methods. To further investigate the spectral radius

611 influence on accuracy, ρ = 0.5 is studied below.

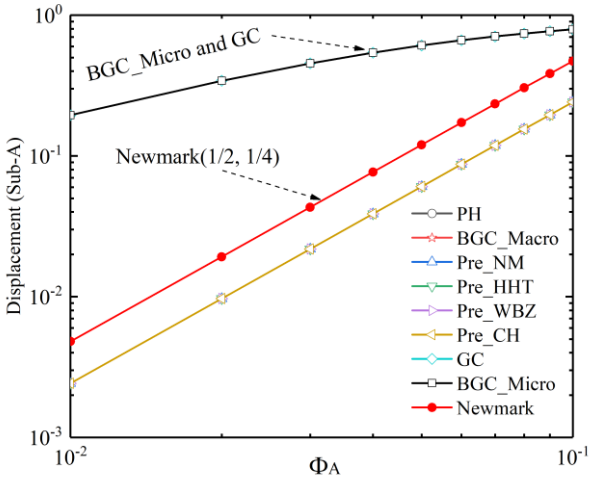

612

613 (a) Displacement errors of Sub_A

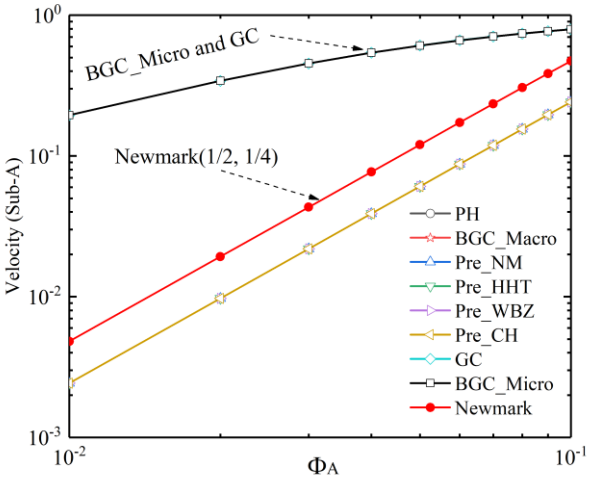

(b) Velocity errors of Sub_A

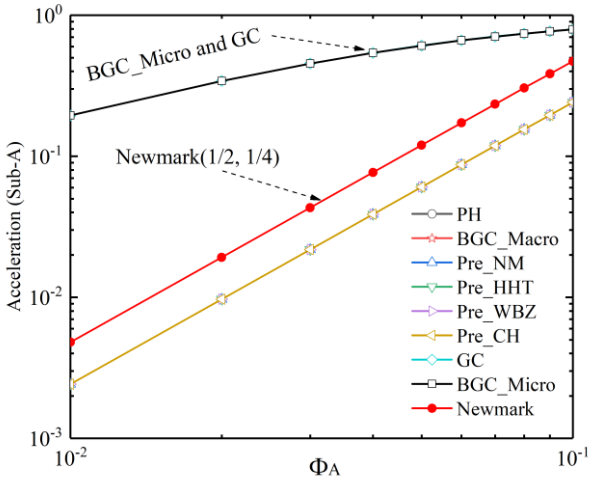

614

615 (c) Acceleration errors of Sub_A

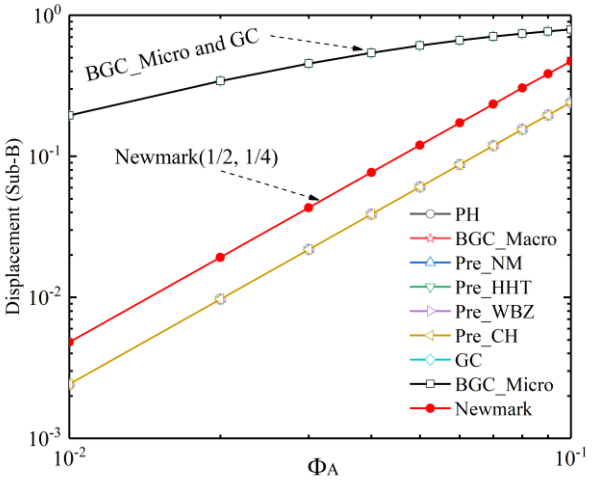

(d) Displacement errors of Sub_B

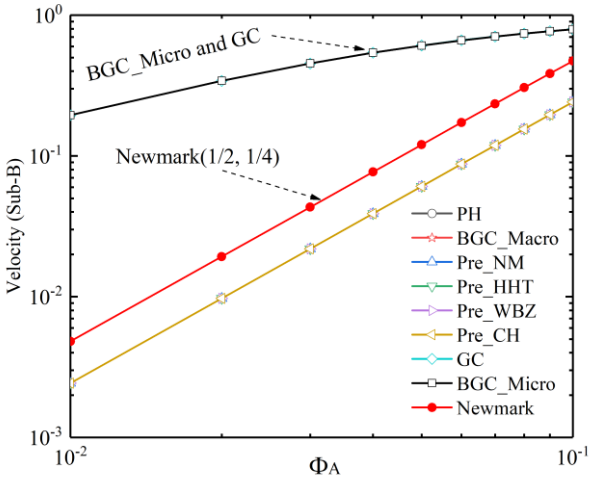

616

617 (e) Velocity errors of Sub_B

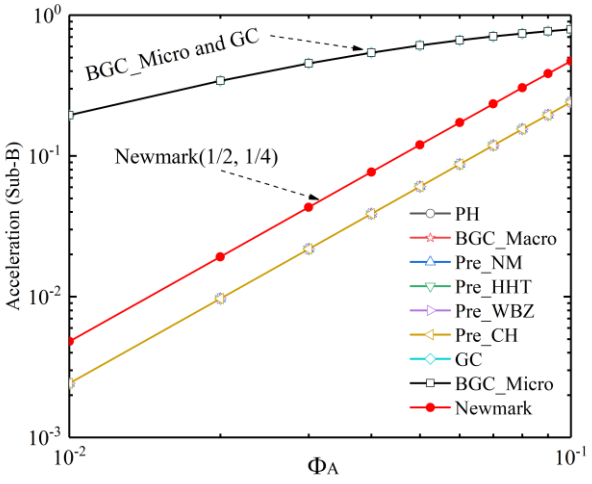

(f) Acceleration errors of Sub_B

618 Fig. 6. Accuracy property varying with time step size for various integration schemes (ρ = 1,

and m = 10)

Note that the reduced angular frequency [11] $\Phi_A = 2\pi \frac{h_A}{T}$ is introduced to simplify the abscissa, the time step size of Sub_A varies from $h_A = 10^{-6}$ s to $h_A = 10^{-7}$ s, corresponding Φ_A ranges from 10^{-1} to 10^{-2}.

To further investigate spectral radius influence on accuracy, absolute error curves of different coupling methods with ρ = 0.5 are shown in Fig. 7. It shows that absolute errors of all quantities increase with Φ_A for all coupling methods. All quantities solved by coupling methods have smaller YP than that of errors solved by CH, HHT, and WBZ, as indicated in Fig. 7. Moreover, Sub_B with micro time step (h_A/m) is much more accurate than that of Sub_A with macro time step. Thus, the seven schemes incorporated the proposed method, i.e., NM scheme and NG schemes, could ensure the second-order accuracy.

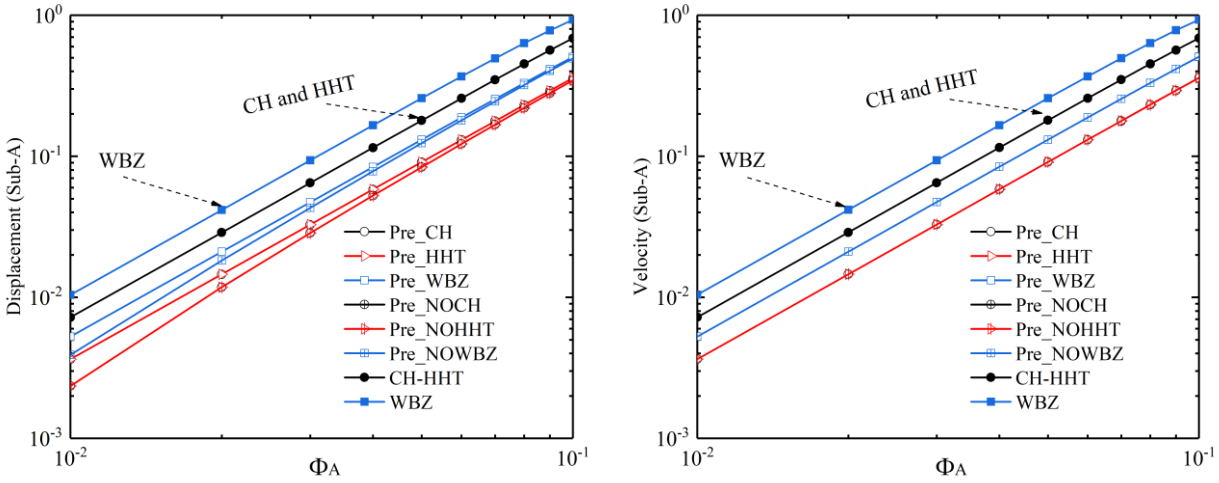

(a) Displacement errors of Sub_A (b) Velocity errors of Sub_A

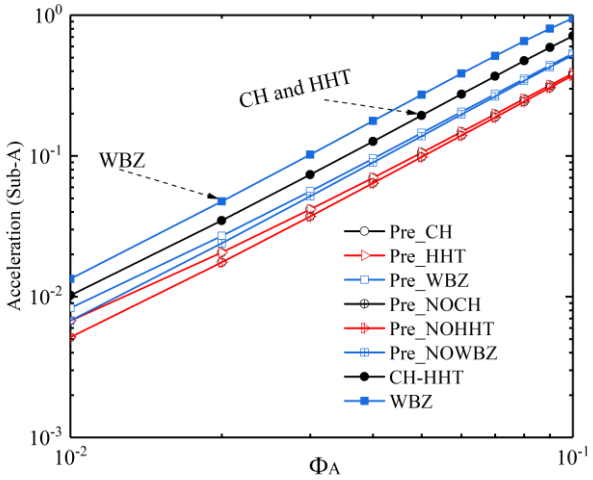

(c) Acceleration errors of Sub_A

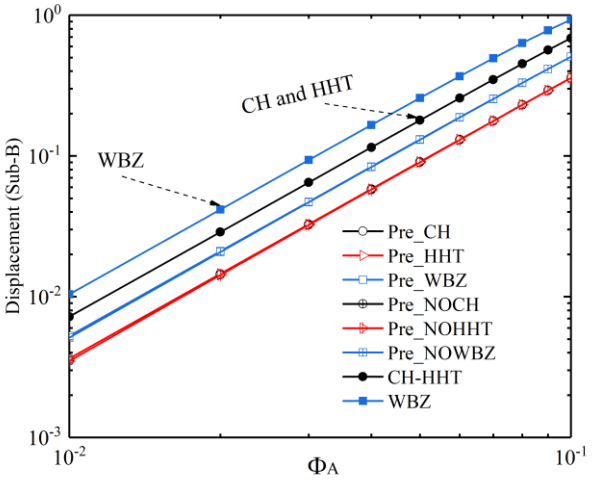

(d) Displacement errors of Sub_B

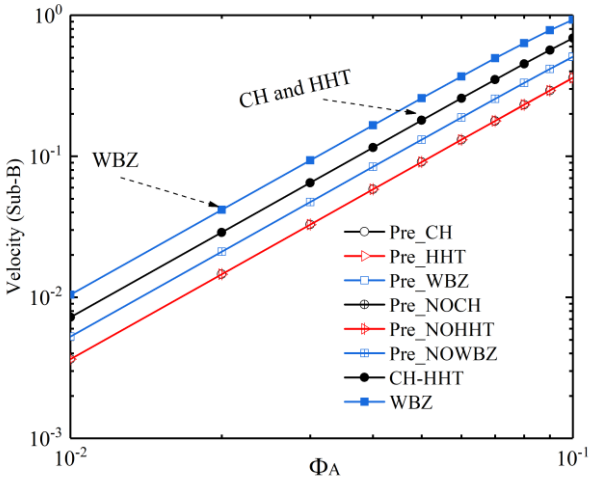

(e) Velocity errors of Sub_B

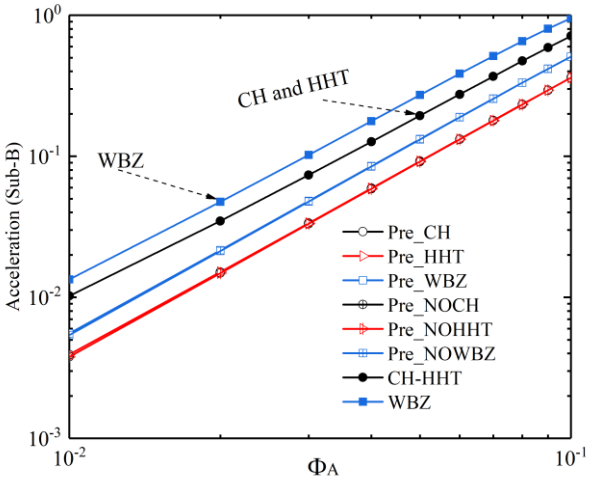

(f) Acceleration errors of Sub_B

Fig. 7. Accuracy property varying with the time step size, (ρ = 0.5, and m = 10)

Note that CH, HHT, and WBZ with ρ = 0.5 and the macro time step are used to calculate the entire oscillator for the purpose of accuracy comparison. CH and HHT have same integration schemes for ρ = 0.5.

Various time step ratios

To study accuracy varying with the time step ratio m, the range of m from 1 to 500 is investigated, and error curves are plotted in Fig. 8. It indicates that for the energy conservative coupling methods, due to more accurate link forces solved by Sub_B with micro time step,

accuracy gradually increases with m for all quantities, and YP is less than that of Newmark. Therefore, the energy conservative coupling methods retain the second-order accuracy. On the contrary, due to energy dissipation at interfaces, absolute errors gradually increase with m for BGC_Micro and GC, and both methods cannot guarantee the second-order accuracy. Furthermore, when $m \geqslant 10$, YP of all computed quantities have small fluctuations with m for the energy conservative methods. Hence, for the energy conservative methods, accuracy of the subdomain with macro time steps can be determined by adjusting m, and high-frequency vibrations or nonlinear behaviors can be easily captured in the subdomain with micro time steps by adjusting m.

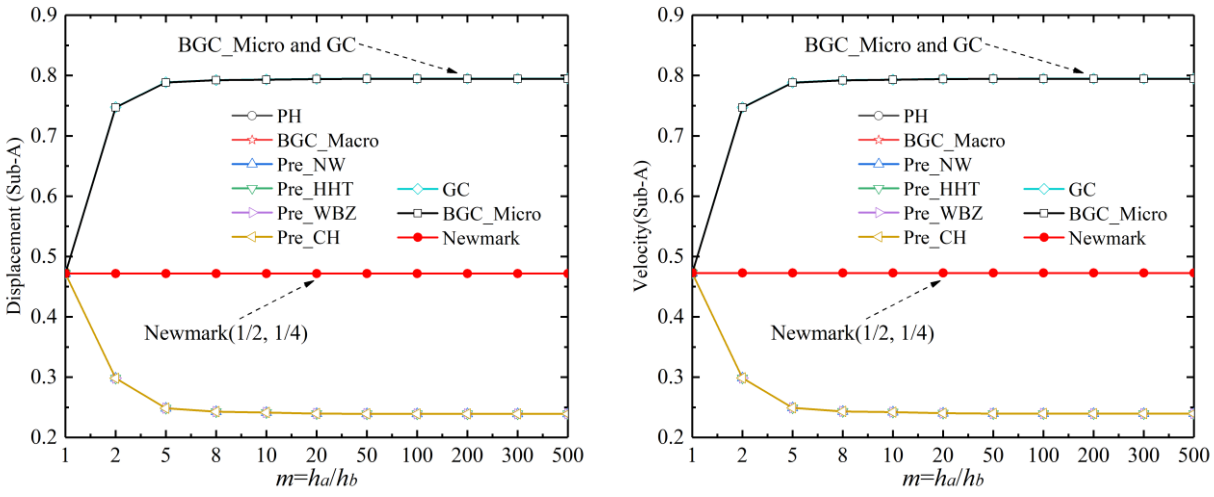

(a) Displacement errors of Sub_A (b) Velocity errors of Sub_A

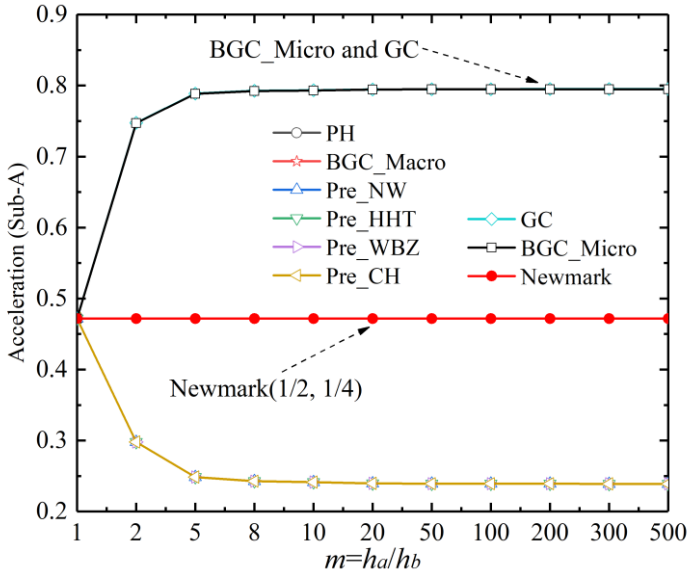

(c) Acceleration errors of Sub_A

Fig. 8. Accuracy property varying with the time step ratio m for various schemes (ρ = 1)

Note that the time step size of Sub_A and Sub_B are set as h_A=1 × 10^{-6} s and $h_B = h_A/m$, respectively. The constant time step h_A is employed in Newmark, hence, its absolute errors are constant. Sub_B with the micro time step has more accurate results, thus, only error curves for Sub_A with large YP is presented in the figure.

To further investigate the spectral radius influence on accuracy, absolute error curves of the integration schemes with ρ = 0.5 are shown in Fig. 9. Similar trends are shown in the figure. More specifically, accuracy gradually increases with m for all computed quantities, the presented coupling method with schemes have smaller YP than that of CH, HHT, and WBZ, as marked in Fig. 9. Thus, the proposed method maintains the second-order accuracy. Furthermore, absolute errors of all computed quantities have small fluctuations when $m \geqslant 10$. Hence, the accuracy of the subdomain with the macro time step can be adjusted by m, and high-frequency vibrations or nonlinear behaviors can be easily captured in the subdomain with micro time step by adjusting m. Note that the second-order accuracy is retained in NG schemes and desirable

algorithmic damping is presented in NG schemes, which can be used to filter spurious vibration contents.

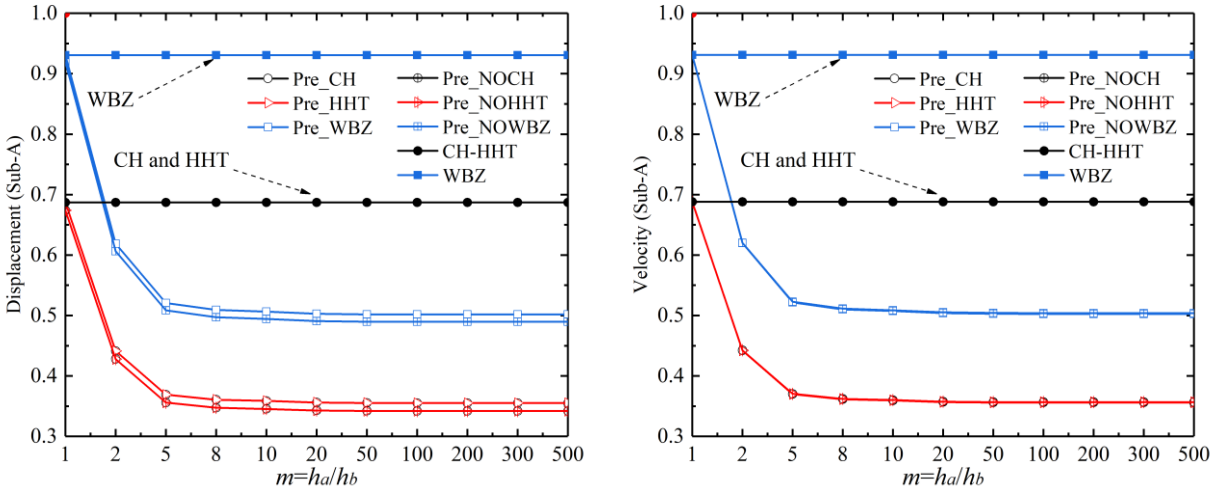

(a) Displacement errors of Sub_A (b) Velocity errors of Sub_A

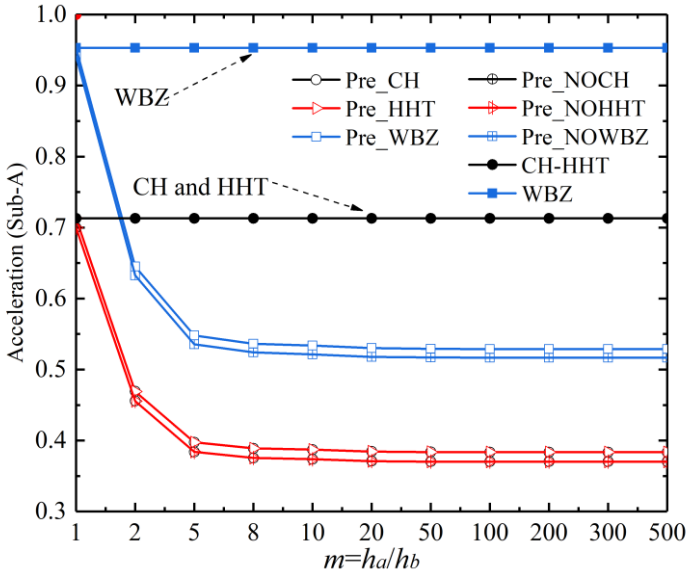

(c) Acceleration errors of Sub_A

Fig. 9. Accuracy property varying with m for various integration schemes (ρ = 0.5)

Note that the time step size of Sub_A and Sub_B are set as h_A=1 × 10^{-6} s and $h_B = h_A/m$, respectively. CH, HHT, and WBZ with ρ = 0.5 and constant macro time step h_A are used to calculate the entire oscillator for the purpose of accuracy comparison.

Various algorithmic parameters

To investigate accuracy property under different algorithmic parameters β, error curves with algorithmic parameters β (γ = 1/2) are indicated in Fig. 10. Note that Newmark with parameter β = 1/12 has the third-order accuracy [5]. It shows that Newmark with (β = 1/12.8 to 1/11.2) has higher accuracy than that of the energy conservative coupling methods. Therefore, more accurate link forces are provided by Sub_B with a micro time step, while the third-order accuracy cannot be obtained for the energy conservative coupling methods. Moreover, YP of two subdomains gradually increases from β = 1/12 to the two sides for the energy conservative coupling methods. The absolute errors of each subdomain can be adjusted by using its own integration parameters.

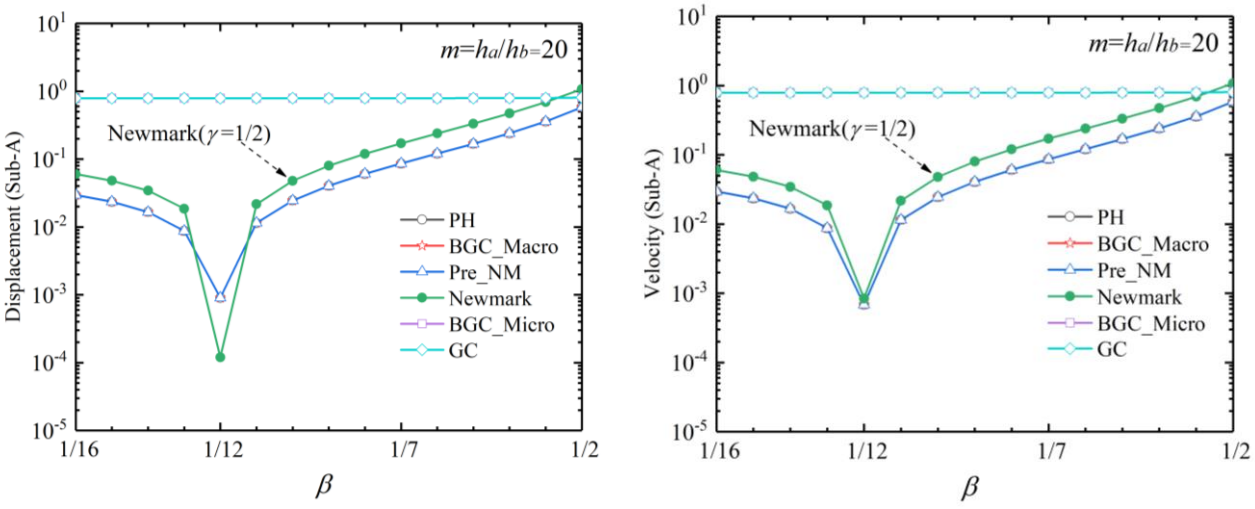

(a) Displacement errors of Sub_A (b) Velocity errors of Sub_A

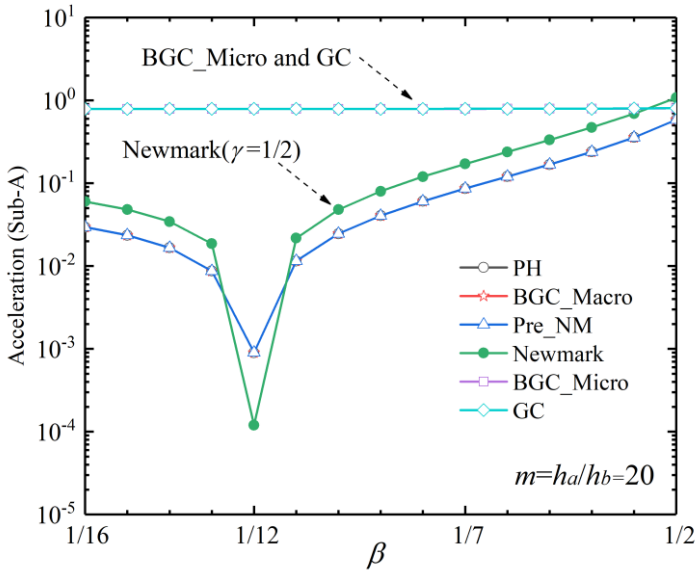

(c) Acceleration errors of Sub_A

Fig. 10. Accuracy property varying with algorithmic parameter (ρ = 1, and m = 20)

Note that the time steps of Sub_A and Sub_B are set as $h_A = 10^{-6}$ s and $h = h_A/20$. Newmark with $\gamma = 1/2$ and the macro time step is used to calculate the entire oscillator for the purpose of comparison.

To further investigate accuracy property under various spectral radius ρ, error curves with various ρ are plotted in Fig. 11. It shows that the developed coupling schemes have more accuracy than that of CH, HHT, and WBZ for all computed quantities. Accuracy increases with ρ for the developed schemes. In other words, the small spectral radius can be used to filter high-frequency spurious vibration contents by using large algorithmic damping (ρ).

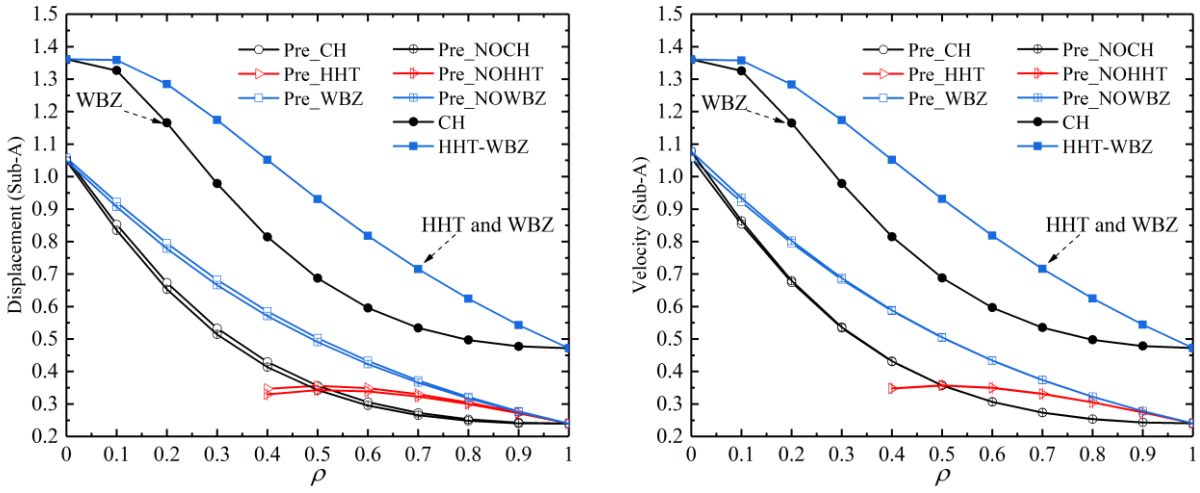

(a) Displacement errors of Sub_A (b) Velocity errors of Sub_A

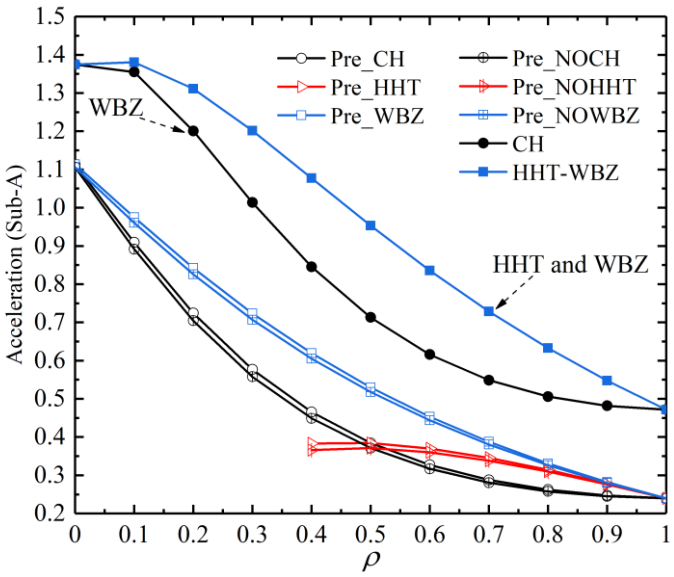

(c) Acceleration errors of Sub_A

Fig. 11. Accuracy property varying with ρ for various integration schemes ($m = 20$)

Note that step sizes of Sub_A and Sub_B are set as $h_A = 10^{-6}$ s and $h = h_A/20$, respectively. CH, HHT, and WBZ with various ρ and constant macro time step h_A are used to calculate the entire oscillator for the purpose of accuracy comparison.

6.2 An oscillator divided into three subdomains

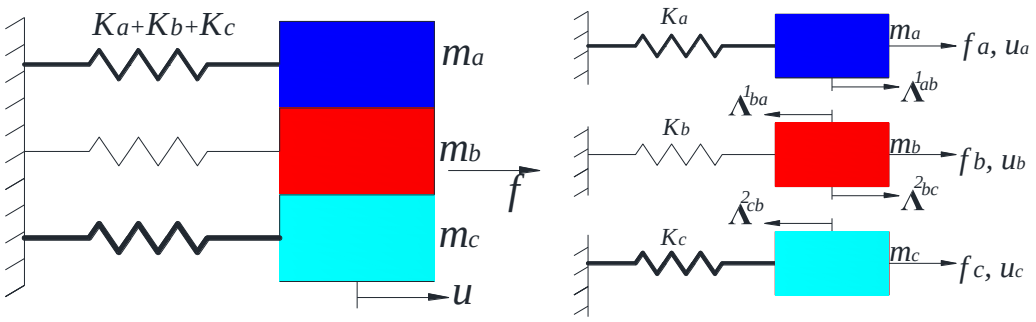

(a) entire oscillator (b) split oscillator

Fig. 12. An oscillator split into three subdomains

Note that mass and stiffness of Sub_A, Sub_B, and Sub_C are ($Ma = Mb = Mc = 1 \times 10^{-6}$) and ($Ka = 4 \times 10^{4}$, $Kb = 1 \times 10^{2}$, and $Kc = 2.5 \times 10^{5}$), respectively. The time steps for three subdomains are $h_A = 5 \times 10^{-8}$ s, $h_B = 1 \times 10^{-7}$ s, and $h_C = 5 \times 10^{-7}$ s. Corresponding ratios are $h_B / h_A = 2$ and $h_C / h_B = 5$. Simulation time is 0.01 s.

To demonstrate the application of multiple subdomains ($\geqslant 3$), the oscillator split into three subdomains is investigated and corresponding calculation information is given in Fig. 12. Only the presented method can be employed to calculate multiple subdomains ($\geqslant 3$) easily, thus, the developed method, Newmark, and theory solutions are employed to solve the coupling system. The solving method of link forces is given in Appendix I for the proposed method with Newmark scheme. Structural responses from 0.00998 *s* to 0.01 *s* are compared in Fig. 13. As observed, structural responses of three subdomains are overlapped with each other for each integration scheme. Responses solved by Pre_NW ($\rho = 1$) are most close to results solved by Newmark and theorical solutions. Compared with Pre_CH and Pre_HHT with $\rho = 0.5$, algorithmic dissipation is dominated for Pre_WBZ with $\rho = 0.5$. Therefore, accurate results can be obtained by using the developed method with $\rho = 1$, and it is easier to filter the high-frequency spurious vibrations by using Pre_WBZ with $\rho = 0.5$.

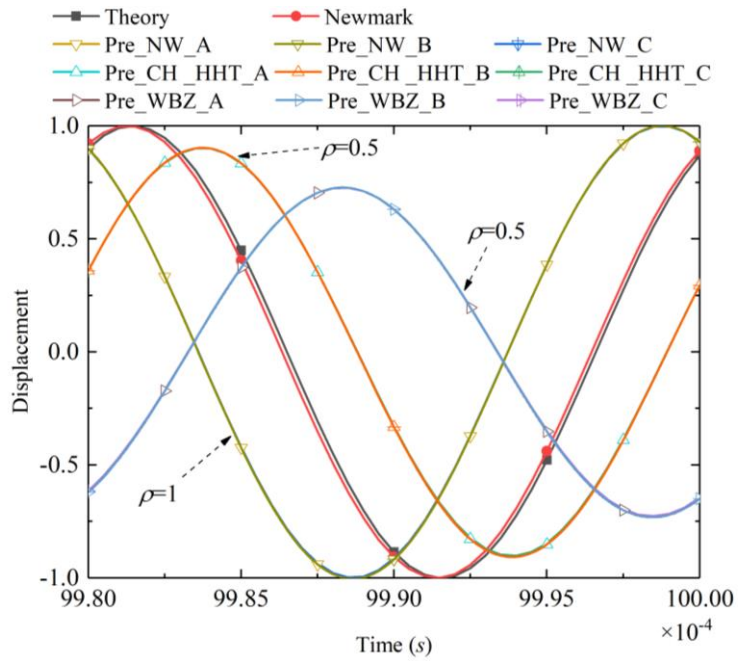

735

736 (a) Displacement

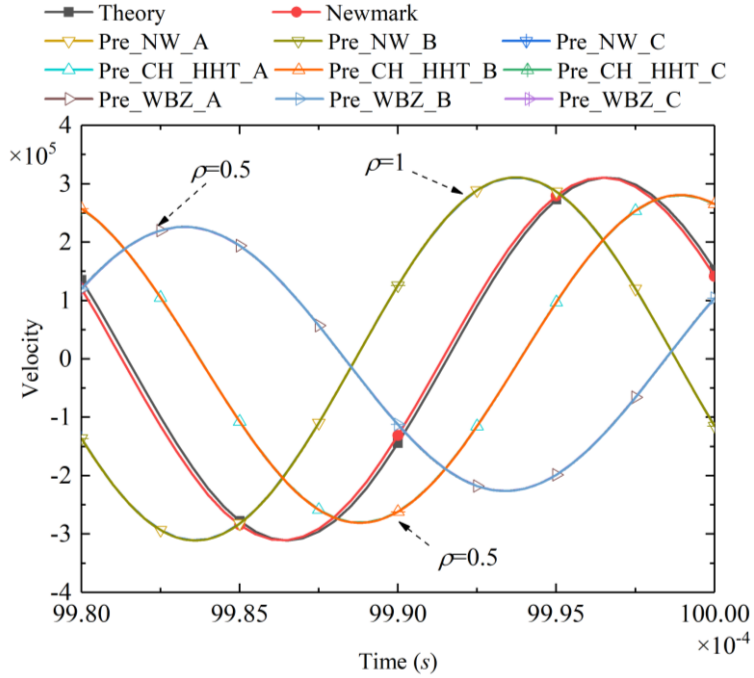

737

738 (b) Velocity

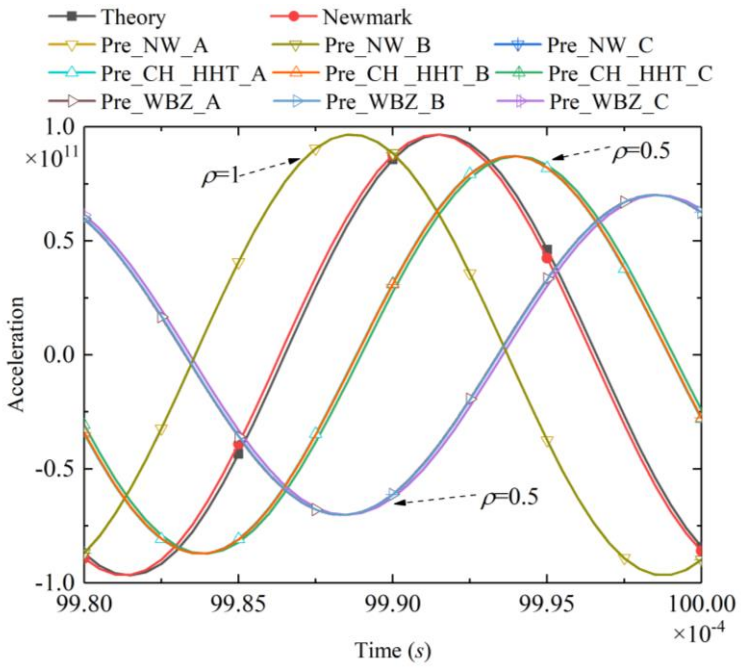

(c) Acceleration

Fig. 13. Structural responses of the oscillator split into three subdomains

Note that theory results are solved by using Eq. (88). Newmark with (1/2, 1/4) is used to calculate the entire oscillator for the purpose of comparison. The time step $h = 5 \times 10^{-7}$ s is employed in theory results and Newmark.

6.3 A wellbore structure

To investigate the accuracy and computational efficiency for a multi-DOF system, a wellbore structure, as depicted in Fig. 14 (a), is calculated by using FEM under the plane strain assumption. To simplify the modeling process, only Pi/36 rad of the wellbore structure is modeled and the relevant parameters are given in Table 2. The radial force defined in the following Eq. (91) is applied on the inner wall and the outer wall is fixed, as shown in Fig. 14 (a). The wellbore structure, as given in Fig. 14 (b), is only decomposed into two subdomains for comparison with other existing integration methods. The time steps of Sub_A and Sub_B are set as 5e-7 *s* and 5e-8 *s*, respectively, corresponding ratio $m = 10$. The lump mass matrix is

used in the calculation. The simulation time is $T = 0.01$ s. Compared with existing methods, the accuracy and computational efficiency are successively discussed in the following sections.

$$\begin{cases} F(t) = f_0 \sin(\omega t) \\ f_0 = 1e5 \\ \omega = 10\pi \end{cases} \tag{91}$$

Table 2 Calculation parameters

Item	Value (Unit)
Modulus of elasticity (EX)	2.0×10^{11} N/m^2
Poisson's ratio (PRXY)	0.3
Density	7850 kg/m^3
Outer diameter (R)	5 m
Inside diameter (r)	0.5 m
Angle	Pi/36 rad

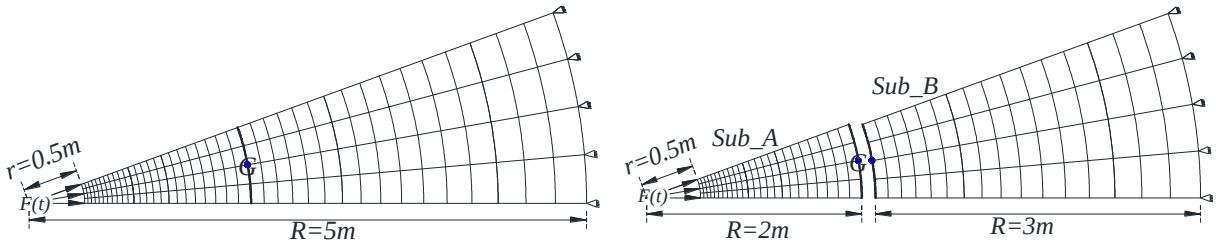

(a) The entire wellbore structure (b) The partitioned wellbore structure.

Fig. 14. Wellbore structure (Pi/36 rad)

1) *Evaluation of accuracy*

To assess the accuracy of various coupling methods, acceleration responses of the interconnected point G, as shown in Fig. 14 (b), are presented in Fig. 15. The entire model is calculated by using Newmark with the unique time step 1e-9 s, and responses of G are considered as reference. As observed, structural responses of two subdomains are overlapped with each other for all schemes. Since Pre_NW and BGC_Macro have the same displacement and velocity integration schemes, as marked in Fig. 15 (b), response curves are overlapped.

Same observation is captured in GC and BGC_Micro. Due to different amplitude decay and period elongation [3][4][5], structural responses solved by using the presented different schemes have a slight difference. Furthermore, different algorithmic dissipations for high-frequency spurious vibration generated by special discretization are presented in the developed schemes.

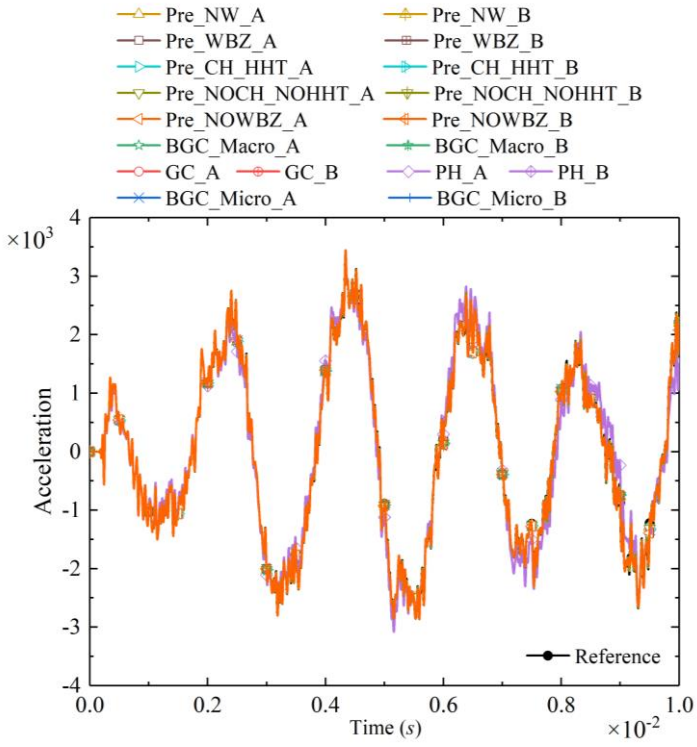

(a) Acceleration responses

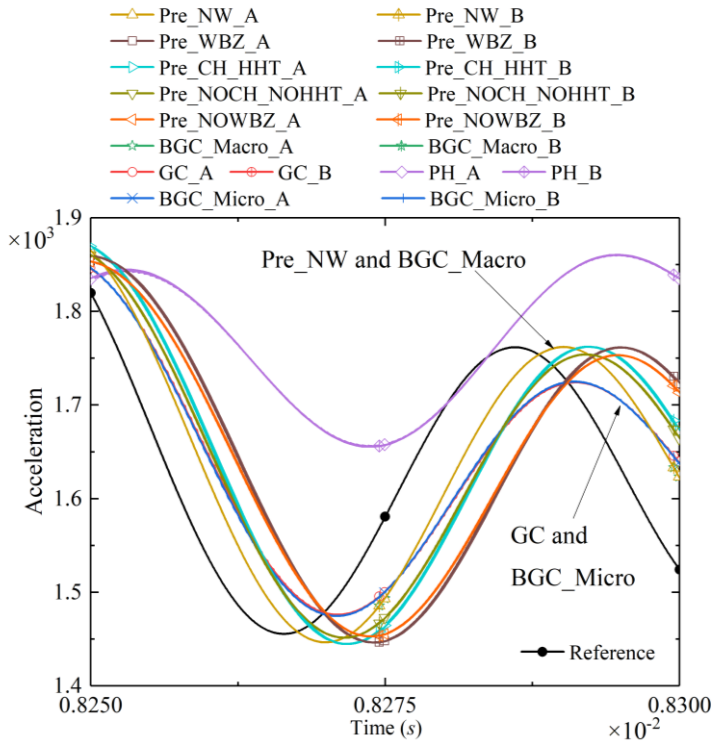

(b) An enlarged view of the acceleration responses within (0.00825 s ~ 0.0083 s)

Fig. 15. Acceleration responses of the point G using different coupling methods (m = 10)

Note that the time step sizes of Sub_A and Sub_B are set as h_A=5 × 10^{-7} s and $h_B = h_A/10$, respectively. The algorithmic parameter (1/2, 1/4) (i.e., ρ = 1) is employed in BGC_Macro, PH, GC, and BGC_Micro. ρ = 0.5 is used in NG schemes, i.e., Pre_CH, Pre_HHT, Pre_WBZ, Pre_NOCH, Pre_NOHHT, Pre_NOWBZ.

2) Evaluation of efficiency

The computational time of various coupling methods is indicated in Fig. 12. Except for the developed decoupling method, each subdomain is split into the free vibration and link vibration for other coupling methods [50][52]. Due to repeated factorizations of "effective stiffness/mass matrix" [4] for two subdomains, especially, the subdomain with micro time steps (i.e., multi-sub-step calculations), these methods are not superior in computational time. However, using the proposed method, once computation is required at each time step for all subdomains.

Therefore, the developed method can improve computational efficiency significantly.

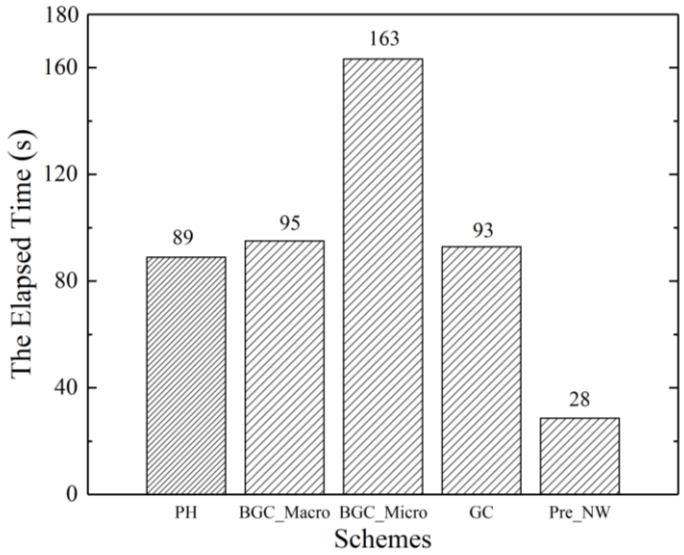

Fig. 16. Computational time of various coupling methods (0.01 s).

Note: A computer equipped with Intel(R) Core (TM) i5 processor and 64 G RAM is employed in the calculation. The parameter setup is consistent with Fig. 15. Computational time is 853 s for the entire model solved by Newmark with unique time step 5e-8 s.

7 Conclusions

In this paper, a decoupling method with energy conservative property is proposed to solve a coupling dynamic system with multiple subdomains and time steps efficiently. The method incorporates New General-α integration schemes with desirable algorithmic damping to filter spurious high-frequency vibration contents and retain the second-order accuracy simultaneously. Three representative examples are studied in terms of accuracy, energy conservation, computational efficiency, and adaptability for multi-subdomains ($\geqslant 3$).

The proposed method can decompose the coupling multi-subdomain system into several independent subdomains with different time steps. Different integration schemes are employed to solve each subdomain independently. Accuracy and stability for each decoupling subdomain can be ensured in solved results by adjusting its own integration parameters. It is convenient to

809 extend to multi-subdomain systems, and an example with three subdomains is calculated for
810 the first time by using the proposed method.

811 Furthermore, due to the independence of each subdomain, different time steps and
812 integration schemes (explicit or implicit) of different subdomains are determined by
813 considering frequency contents, applied loads, and possible nonlinear behaviors of each
814 subdomain. Therefore, the unconditional stability of the implicit scheme and high efficiency of
815 the explicit scheme are retained in the solving process simultaneously. Compared with other
816 existing multi-time-step methods, vibrations are not split into link vibrations and free vibrations
817 for all subdomains. In other words, each subdomain under link forces and external forces is
818 calculated only once for each time step. Therefore, computational efficiency is improved
819 significantly.

820 General-α schemes are covered to the proposed method, thus, desirable algorithmic damping
821 can be employed to filter high-frequency spurious vibration contents, which generate by spatial
822 discretization. Simultaneously, the second-order accuracy is ensured in numerical results, while
823 the third-order accuracy cannot be obtained. Moreover, accuracy of each subdomain can be
824 determined by adjusting the time step ratio m and it has small fluctuations when $m \geqslant 10$.
825 Therefore, high-frequency vibrations or nonlinear behaviors can be easily captured in the
826 subdomain with a micro time step by adjusting m.

827

828 **Appendix I. Calculation of Link forces for a system with three subdomains**

829 In this section, two-two interconnected three-subdomain (A, B, C) coupling system with
830 different time steps, as shown in Fig. A1, are selected to illustrate the computational process of

link forces by using Pre_NW. Dynamic equations of the coupling system are written as:

$$\mathbb{K}^{*\mathrm{A}}\Delta\mathbb{U}_{i_a}^{A}+\boldsymbol{L}_1^{A_B\,T}\Delta\boldsymbol{\Lambda}_{i_a}^{1_{ab}}=\mathbb{F}_{i_a}^{A}\qquad\forall i_a\in\{1,m_a\}\tag{I-1a}$$

$$\mathbb{K}^{*\mathrm{B}}\Delta\mathbb{U}_{i_b}^{B}+\boldsymbol{L}_1^{B_A\,T}\Delta\boldsymbol{\Lambda}_{i_b}^{1_{ba}}+\boldsymbol{L}_2^{B_C\,T}\Delta\boldsymbol{\Lambda}_{i_b}^{2_{bc}}=\mathbb{F}_{i_b}^{B}\qquad\forall i_b\in\{1,m_b\}\tag{I-1b}$$

$$\mathbb{K}^{*\mathrm{C}}\Delta\mathbb{U}_{i_c}^{C}+\boldsymbol{L}_2^{C_B\,T}\Delta\boldsymbol{\Lambda}_{i_c}^{2_{cb}}=\mathbb{F}_{i_c}^{C}\qquad\forall i_c\in\{1,m_c\}\tag{I-1c}$$

where m_a, m_b, and m_c refer to the number of time steps for subdomains A, B, and C, respectively. The system time step is set as ΔT. Two continuity velocity conditions built at t_m are acted on the interfaces AB and BC, which can be written as follows:

$$\boldsymbol{L}_1^{A_B}\boldsymbol{v}_{t_m}^{A}+\boldsymbol{L}_1^{B_A}\boldsymbol{v}_{t_m}^{B}=0\tag{I-2a}$$

$$\boldsymbol{L}_2^{B_C}\boldsymbol{v}_{t_m}^{B}+\boldsymbol{L}_2^{C_B}\boldsymbol{v}_{t_m}^{C}=0\tag{I-2b}$$

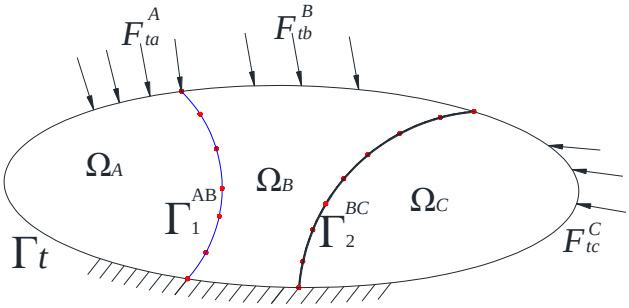

Fig. A1. Two-two interconnected three subdomain coupling system

Note that Γ_t is boundary conditions; and Γ_1^{AB} denotes the 1^{st} interface interconnected subdomain A and subdomain B.

The above velocity continuity conditions are:

$$\sum_{i_a=1}^{m_a}\boldsymbol{L}_1^{A_B}\left(\Delta\bar{\boldsymbol{v}}_{i_a}^{A}+\Delta\boldsymbol{w}_{i_a}^{A}\right)+\sum_{i_b=1}^{m_b}\boldsymbol{L}_1^{B_A}\left(\Delta\bar{\boldsymbol{v}}_{i_b}^{B}+\Delta\boldsymbol{w}_{i_b}^{B}\right)=0\tag{I-3a}$$

$$\sum_{i_b=1}^{m_b}\boldsymbol{L}_2^{B_C}\left(\Delta\bar{\boldsymbol{v}}_{i_b}^{B}+\Delta\boldsymbol{w}_{i_b}^{B}\right)+\sum_{i_c=1}^{m_c}\boldsymbol{L}_2^{C_B}\left(\Delta\bar{\boldsymbol{v}}_{i_c}^{C}+\Delta\boldsymbol{w}_{i_c}^{C}\right)=0\tag{I-3b}$$

The interface link force increments are identical for interconnected subdomains within the system time step, and the linear interpolation of link forces is assumed in time sub-steps. Therefore, for the 1^{st} interface Γ_1^{AB} interconnected subdomains A and B, by using the

interface link forces at the system time step t_m, link forces at micro time sub-steps can be calculated as:

$$\Delta\boldsymbol{\Lambda}^{1_{ab}} = \Delta\boldsymbol{\Lambda}^{AB_1}_{t_m} / m_a \tag{I-4a}$$

$$\Delta\boldsymbol{\Lambda}^{1_{ba}} = \Delta\boldsymbol{\Lambda}^{AB_1}_{t_m} / m_b \tag{I-4b}$$

Note that the right item of Eq. (I-4) at all time sub-steps is constant, hence, its subscript is ignored. Similar treatment is performed for the 2^{nd} interface Γ_2^{BC} interconnected subdomains B and C, link forces at micro time steps are:

$$\Delta\boldsymbol{\Lambda}^{2_{bc}} = \Delta\boldsymbol{\Lambda}^{BC_2}_{t_m} / m_b \tag{I-5a}$$

$$\Delta\boldsymbol{\Lambda}^{2_{cb}} = \Delta\boldsymbol{\Lambda}^{BC_2}_{t_m} / m_c \tag{I-5b}$$

For three subdomains under link forces, using Eq. (32c), the velocity increments at each time step can be calculated as follows:

$$\Delta\boldsymbol{w}^A_{i_a} = -\boldsymbol{K}^{*\text{-}1}_A \boldsymbol{L}_1^{A_B{}^T} \Delta\boldsymbol{\Lambda}^{1_{ab}} \tag{I-6a}$$

$$\Delta\boldsymbol{w}^B_{i_b} = -\boldsymbol{K}^{*\text{-}1}_B \left(\boldsymbol{L}_1^{B_A{}^T} \Delta\boldsymbol{\Lambda}^{1_{ba}} + \boldsymbol{L}_2^{B_C{}^T} \Delta\boldsymbol{\Lambda}^{2_{bc}} \right) \tag{I-6b}$$

$$\Delta\boldsymbol{w}^C_{i_c} = -\boldsymbol{K}^{*\text{-}1}_C \boldsymbol{L}_2^{C_B{}^T} \Delta\boldsymbol{\Lambda}^{2_{cb}} \tag{I-6c}$$

Substituting Eq. (I-6) into Eq. (I-3), two velocity continuity conditions can be written as:

$$\begin{aligned} &\sum_{i_a=1}^{m_a} \boldsymbol{L}_1^{A_B} \Delta\bar{\boldsymbol{v}}^A_{i_a} + \sum_{i_b=1}^{m_b} \boldsymbol{L}_1^{B_A} \Delta\bar{\boldsymbol{v}}^B_{i_b} = \\ &\sum_{i_a=1}^{m_a} \boldsymbol{L}_1^{A_B} \boldsymbol{K}^{*\text{-}1}_A \boldsymbol{L}_1^{A_B{}^T} \Delta\boldsymbol{\Lambda}^{1_{ab}} + \\ &\sum_{i_b=1}^{m_b} \boldsymbol{L}_1^{B_A} \boldsymbol{K}^{*\text{-}1}_B \left(\boldsymbol{L}_1^{B_A{}^T} \Delta\boldsymbol{\Lambda}^{1_{ba}} + \boldsymbol{L}_2^{B_C{}^T} \Delta\boldsymbol{\Lambda}^{2_{bc}} \right) \end{aligned} \tag{I-7a}$$

$$\sum_{i_b=1}^{m_b} \boldsymbol{L}_2^{B_C} \Delta \bar{\boldsymbol{v}}_{i_b}^{B} + \sum_{i_c=1}^{m_c} \boldsymbol{L}_2^{C_B} \Delta \bar{\boldsymbol{v}}_{i_c}^{C} =$$

867
$$\sum_{i_b=1}^{m_b} \boldsymbol{L}_2^{B_C} \boldsymbol{K}_B^{*-1} \left(\boldsymbol{L}_1^{B_A{}^T} \Delta \boldsymbol{\Lambda}^{1ba} + \boldsymbol{L}_2^{B_C{}^T} \Delta \boldsymbol{\Lambda}^{2bc} \right) + \tag{I-7b}$$

$$\sum_{i_c=1}^{m_c} \boldsymbol{L}_2^{C_B} \boldsymbol{K}_C^{*-1} \boldsymbol{L}_2^{C_B{}^T} \Delta \boldsymbol{\Lambda}^{2cb}$$

868 Substituting link forces and velocity generated by external excitations (i.e., Eqs. (I-4), (I-5),

869 and (46)) into Eq. (I-7), one has:

$$\boldsymbol{L}_1^{A_B} \Delta \bar{\boldsymbol{V}}^{A} + \boldsymbol{L}_1^{B_A} \Delta \bar{\boldsymbol{V}}^{B} =$$

870
$$\left(\frac{1}{m_a} \sum_{i_a=1}^{m_a} \boldsymbol{L}_1^{A_B} \boldsymbol{K}_A^{*-1} \boldsymbol{L}_1^{A_B{}^T} + \frac{1}{m_b} \sum_{i_b=1}^{m_b} \boldsymbol{L}_1^{B_A} \boldsymbol{K}_B^{*-1} \boldsymbol{L}_1^{B_A{}^T} \right) \Delta \boldsymbol{\Lambda}_{t_{n+1}}^{AB_1} + \tag{I-8a}$$

$$\frac{1}{m_b} \sum_{i_b=1}^{m_b} \boldsymbol{L}_1^{B_A} \boldsymbol{K}_B^{*-1} \boldsymbol{L}_2^{B_C{}^T} \Delta \boldsymbol{\Lambda}_{t_{n+1}}^{BC_2}$$

$$\boldsymbol{L}_2^{B_C} \Delta \bar{\boldsymbol{V}}^{B} + \boldsymbol{L}_2^{C_B} \Delta \bar{\boldsymbol{V}}^{C} = \frac{1}{m_b} \sum_{i_b=1}^{m_b} \boldsymbol{L}_2^{B_C} \boldsymbol{K}_B^{*-1} \boldsymbol{L}_1^{B_A{}^T} \Delta \boldsymbol{\Lambda}_{t_{n+1}}^{AB_1}$$

871
$$+ \left(\frac{1}{m_b} \sum_{i_b=1}^{m_b} \boldsymbol{L}_2^{B_C} \boldsymbol{K}_B^{*-1} \boldsymbol{L}_2^{B_C{}^T} + \frac{1}{m_c} \sum_{i_c=1}^{m_c} \boldsymbol{L}_2^{C_B} \boldsymbol{K}_C^{*-1} \boldsymbol{L}_2^{C_B{}^T} \right) \Delta \boldsymbol{\Lambda}_{t_{n+1}}^{BC_2} \tag{I-8b}$$

872 For simplification, Eq. (I-8) is rewritten as follows:

873
$$\bar{\boldsymbol{V}}_{AB} = \boldsymbol{H}_{AB} \Delta \boldsymbol{\Lambda}_{t_{n+1}}^{AB_1} + \boldsymbol{H}_{AC_2} \Delta \boldsymbol{\Lambda}_{t_{n+1}}^{BC_2} \tag{I-9a}$$

874
$$\bar{\boldsymbol{V}}_{BC} = \boldsymbol{H}_{CA_2} \Delta \boldsymbol{\Lambda}_{t_{n+1}}^{AB_1} + \boldsymbol{H}_{BC} \Delta \boldsymbol{\Lambda}_{t_{n+1}}^{BC_2} \tag{I-9b}$$

875 where the coefficients are designed as follows:

876
$$\bar{\boldsymbol{V}}_{AB} = \boldsymbol{L}_1^{A_B} \Delta \bar{\boldsymbol{V}}^{A} + \boldsymbol{L}_1^{B_A} \Delta \bar{\boldsymbol{V}}^{B} \tag{I-10a}$$

877
$$\boldsymbol{H}_{AB} = \frac{1}{m_a} \sum_{i_a=1}^{m_a} \boldsymbol{L}_1^{A_B} \boldsymbol{K}_A^{*-1} \boldsymbol{L}_1^{A_B{}^T} + \frac{1}{m_b} \sum_{i_b=1}^{m_b} \boldsymbol{L}_1^{B_A} \boldsymbol{K}_B^{*-1} \boldsymbol{L}_1^{B_A{}^T} \tag{I-10b}$$

878
$$\boldsymbol{H}_{AC_2} = \frac{1}{m_b} \sum_{i_b=1}^{m_b} \boldsymbol{L}_1^{B_A} \boldsymbol{K}_B^{*-1} \boldsymbol{L}_2^{B_C{}^T} \tag{I-10c}$$

879
$$\bar{\boldsymbol{V}}_{BC} = \boldsymbol{L}_2^{B_C} \Delta \bar{\boldsymbol{V}}^{B} + \boldsymbol{L}_2^{C_B} \Delta \bar{\boldsymbol{V}}^{C} \tag{I-11a}$$

$$\boldsymbol{H}_{CA_2} = \frac{1}{m_b}\sum_{i_b=1}^{m_b} \boldsymbol{L}_2^{B_C}\boldsymbol{K}_B^{*\text{-}1}\boldsymbol{L}_1^{B_A{}^T} \tag{I-11b}$$

$$\boldsymbol{H}_{BC} = \frac{1}{m_b}\sum_{i_b=1}^{m_b} \boldsymbol{L}_2^{B_C}\boldsymbol{K}_B^{*\text{-}1}\boldsymbol{L}_2^{B_C{}^T} + \frac{1}{m_c}\sum_{i_c=1}^{m_c} \boldsymbol{L}_2^{C_B}\boldsymbol{K}_C^{*\text{-}1}\boldsymbol{L}_2^{C_B{}^T} \tag{I-11c}$$

It is worth noting that for a linear system, except for Eqs. (I-10a) and (I-11a), other coefficients are constant, which can be given before calculation. According to the principle of the calculus of algebraic equations, two link forces can be calculated as follow:

$$\Delta\boldsymbol{\Lambda}_{t_{n+1}}^{AB_1} = \left(\boldsymbol{H}_{CA_2} - \boldsymbol{H}_{BC}\boldsymbol{H}_{AC_2}^{-1}\boldsymbol{H}_{AB}\right) \backslash \left(\bar{\boldsymbol{V}}_{BC} - \boldsymbol{H}_{BC}\boldsymbol{H}_{AC_2}^{-1}\bar{\boldsymbol{V}}_{AB}\right) \tag{I-12a}$$

$$\Delta\boldsymbol{\Lambda}_{t_{n+1}}^{BC_2} = \boldsymbol{H}_{BC} \backslash \left(\bar{\boldsymbol{V}}_{BC} - \boldsymbol{H}_{CA_2}\Delta\boldsymbol{\Lambda}_{t_{n+1}}^{AB_1}\right) \tag{I-12b}$$

Appendix II Procedure of the proposed decoupling method

The integration procedure of Pre_NM is indicated in Table 3:

Table 3 Calculation flowchart of Pre_NM

(1) Calculate matrices and parameters

$\boldsymbol{K}_A, \boldsymbol{M}_A, \boldsymbol{L}_A^T, \gamma_A, \beta_A, h_A$ $\quad$ $\boldsymbol{K}_B, \boldsymbol{M}_B, \boldsymbol{L}_B^T, \gamma_B, \beta_B, h_B$

$\boldsymbol{K}_A^* = \frac{1}{\gamma_A h_A}\boldsymbol{M}_A + \frac{h_A\beta_A}{\gamma_A}\boldsymbol{K}_A$ $\quad$ $\boldsymbol{K}_B^*, \boldsymbol{GG}, (\boldsymbol{b}_i, \boldsymbol{A}_i \ \ (i = 1,,,m))$

(2) Given initial conditions and condensed matrix

$\mathbb{U}_0^A,\ \mathbb{U}_0^B,\ \boldsymbol{H}_2 = m\boldsymbol{L}^A\boldsymbol{K}_A^{*\text{-}1}\boldsymbol{L}_A^T + \boldsymbol{L}^B\boldsymbol{b}_1\boldsymbol{L}_B^T$

(3) Calculate link forces

$$\boldsymbol{DV}_2 = \boldsymbol{L}_A\boldsymbol{K}_A^{*\text{-}1}\boldsymbol{P}_m^A + \boldsymbol{L}_B\left(\boldsymbol{b}_1\boldsymbol{K}^*\Delta\bar{\boldsymbol{v}}_1^B + \sum_{j=1}^{m-1}\boldsymbol{b}_{m+1-j}\boldsymbol{F}_j^B\right)$$

$$\Delta\boldsymbol{\Lambda} = \boldsymbol{H}_2 \backslash \boldsymbol{DV}_2$$

(4) Calculate the responses of A and B

$$\begin{cases} \mathbb{K}_A^* \Delta \mathbb{U}_m^A = \mathbb{R}_m^A - \mathbb{N}_A \mathbb{U}_0^A \\ \mathbb{K}_B^* \Delta \mathbb{U}_j^B = \mathbb{R}_j^B - \mathbb{N}_B \mathbb{U}_{j-1}^B \quad \forall j \in \{1, m\} \end{cases}$$

(5) Return to (3) for the next step or stop

References

[1] Bathe KJ. (2006). "Finite element procedures." Prentice Hall.

[2] A. Gravouil1, A. Combescure and M. Brun. Heterogeneous asynchronous time integrators for computational structural dynamics. Int. J. Numer. Methods Eng. 2015; 102:202–232.

[3] P. Yuan, DJ Li, C.S Cai, and G.J. Xu. Time Integration Method with High Accuracy and Efficiency for Structural Dynamic Analysis. Journal of Engineering Mechanics, 2019, 145(3).

[4] P. Yuan, DJ Li, C.S Cai, and G.J Xu. An Efficient Decoupling Dynamic Algorithm for Coupled Multi-Spring-Systems. Computers & Structures. 2018; 209:44-56.

[5] P. Yuan, DJ Li, C.S Cai, and G.J Xu. An Efficient Explicit Integration Method with Third-order Accuracy and Controllable Dissipation and Decoupling Properties. International Journal for Numerical Methods in Engineering.

[6] J.H. Kim, S.H. Boo, P.S. Lee, A dynamic condensation method with free interface substructuring, Mech. Syst. Sig. Process., 129 (2019), 218-234.

[7] M. Gerardin, D. Rixen, Mechanical Vibrations, Theory and Applications to Structural Dynamics, seconded., Wiley, 1997.

[8] K.B. Nakshatrala, A. Prakash, K.D. Hjelmstad, On dual Schur domain decomposition method for linear first-order transient problems, J. Comput. Phys. 228 (2009) 7957–7985.

[9] A. Prakash, K.D. Hjelmstad, A FETI-based multi-time-step coupling method for newmark schemes in structural dynamics, International Journal for Numerical Methods in Engineering 61 (2004) 2183–2204.

[10] N. Mahjoubi, A. Gravouil, A. Combescure, N. Greffet, A monolithic energy conserving method to couple heterogeneous time integrators with incompatible time steps in structural dynamics, Comput. Methods Appl. Mech. Engrg. 200 (2011) 1069–1086.

[11] M. Brun, A. Gravouil, A. Combescure, A. Limam. Two FETI-based heterogeneous time step coupling methods for Newmark and α-schemes derived from the energy method.Comput. Methods Appl. Mech. Engrg. 283 (2015) 130–176

[12] H. BenDhia, Further insights by theoritical investigations of the multiscale arlequin method, Internat. J. Multiscale Comp. Engr. 2008; 6 215-232.

[13] P. Aubertin, J. R´ethor´e, R.D. Borst, Energy conservation of atomistic/continuum coupling, Internat. J. Numer. Methods Engrg. 78 (2009) 1365–1386.

[14] A. Gravouil, A. Combescure, Multi-time-step explicit-implicit method for non-linear structural dynamics, Int. J. Numer. Methods Engrg. 50 (2001) 199–225.

[15] Muller A, Hughes TJR. Mixed finite element methods and iterative solutions: an algorithm for structural finite element analysis. Proceedings of the International Conference on Innovative Methods for Nonlinear Problems, Pineridge Press International Limited: Swansea, U.K., 1984.

[16] Miranda I, Ferencz R.M, Hughes T.J.R. An improved implicit-explicit time integration method for structural dynamics. Earthquake Engineering and Structural Dynamics 1989; 18:643-653.

[17] Belytschko T, Mullen R. Mesh partitions of explicit-implicit time integration. Proceedings US-Germany Symposium on Formulations and Computational Algorithms in Finite Element Analysis, Massachussetts Institute of Technology, Cambridge, MA, 1976.

[18] Belytschko T, Mullen R. Stability of explicit-implicit mesh partitions in time integration. International Journal for Numerical Methods in Engineering 1978; 12:1575-1586.

[19] Hughes T.J.R, Liu W.K. Implicit-explicit finite elements in transient analysis: implementation and numerical examples. Journal of Applied Mechanics 1978; 45:375-378.

[20] Hughes T.J.R, Liu W.K. Implicit-explicit finite elements in transient analysis: stability theory. Journal of Applied Mechanics 1978; 45:371-374.

[21] Hughes T.J.R, Pister K.S, Taylor R.L. Implicit-explicit finite elements in non-linear transient analysis. Computer Methods in Applied Mechanics and Engineering 1979; 17(18):159-182.

[22] Chen G.G, Hsu T.R. A mixed explicit-implicit (EI) algorithm for creep stress analysis. International Journal for Numerical Methods in Engineering 1988; 26:511-524.

[23] Belytschko T, Lu Y.Y. Stability analysis of elemental explicit-implicit partitions by Fourier methods. Computer Methods in Applied Mechanics and Engineering 1992; 95:87-96.

[24] J. Brunetti,W. D'Ambrogio,A. Fregolent, Dynamic coupling of substructures with sliding friction interfaces, Mech. Syst. Sig. Process., 141 (2020), 106731.

[25] P. Smolinski, YS Wu. An implicit multi-time step integration method for structural dynamics problems. Computational Mechanics 22 (1998) 337±343

[26] X. Wang, T.L. Hill, S.A. Neild, A.D. Shaw, H. Haddad Khodaparast, M.I. Friswell, Model updating strategy for structures with localised nonlinearities using frequency response measurements, Mech. Syst. Sig. Process., 100 (2018), 940-961.

[27] Liu W.K, Belytschko T. Mixed-time implicit-explicit finite elements for transient analysis. Computers and Structures 1982; 15:445-450.

[28] P. Smolinski, T. Belytschko, M. Neal, Multi-time-step integration using nodal partitioning, Int. J. Numer. Methods Engrg. 26 (1988) 349-359.

[29] W.J.T. Daniel, Analysis and implementation of a new constant acceleration subcycling algorithm, Int. J. Numer. Methods Engrg. 40 (1997) 2841–2855.

[30] Daniel WJT. The subcycled Newmark algorithm. Computational Mechanics 1997; 20:272–281.

[31] Belytschko T, Gilbersen N.D. Implementation of mixed time integration techniques on a vectorized computer with shared memory. International Journal for Numerical Methods in Engineering 1992; 35:1803-1828.

[32] Belytschko T, Smolinski P, Liu W.K. Multi-stepping implicit-explicit procedures in transient analysis.Proceedings of the International Conference on Innovative Methods for Nonlinear Problems, Pineridge Press. International Limited: Swansea, U.K., 1984.

[33] Park K.C. Partitioned transient analysis procedures for coupled-field problems: stability analysis. Journal of Applied Mechanics 1980; 47:370–376.

[34] W.J.T. Daniel, A study of the stability of subcycling algorithms in structural dynamics, Comput. Methods Appl. Mech. Engrg. 1998; 156 1-13.

[35] T. Belytschko, P. Smolinski, W.K. Liu, Stability of multi-time step partitioned integrators for first-order finite element systems, Comput. Methods Appl. Mech. Engrg. 49 (1985) 281–297.

[36] P. Smolinski, S. Sleith, T. Belytschko, Stability of an explicit multi-time step integration algorithm for linear structural dynamics equations, Comput. Mech. 18 (3) (1996) 236–244.

[37] Liu W.K, Lin J. Stability of mixed time integration schemes for transient thermal analysis. Numerical Heat Transfer 1982; 5:211-222.

[38] T. Belytschko, P. Smolinski, W.K. Liu, Multi-stepping implicit–explicit procedures in transient analysis, in: Proceedings of the International Conference on Innovative Methods for Nonlinear Problems, Pineridge Press International Limited, Swansea, UK, 1984.

[39] W.J.T. Daniel, Explicit/implicit partitioning and a new explicit form of the generalized alpha method, Commun. Numer. Methods Engrg. 19 2003; (11) 909–920.

[40] Farhat C, Roux F.X. A method of finite element tearing and interconnecting and its parallel solution algorithm. International Journal for Numerical Methods in Engineering 1991; 32:1205–1227.

[41] Farhat C, Crivelli L, Roux F.X. A transient FETI methodology for large-scale parallel implicit computations in structural mechanics. International Journal for Numerical Methods in Engineering 1994; 37:1945–1975.

[42] Farhat C, Crivelli L, G´eradin M. Implicit time integration of a class of constrained hybrid formulations. Part I: spectral stability theory. Computer Methods in Applied Mechanics and Engineering 1995; 125:71–107.

995 [43] A. Combescure, A. Gravouil, A numerical scheme to couple subdomains with different
996 time-steps for predominantly linear transient analysis, Comput. Methods Appl. Mech.
997 Engrg. 191 (2002) 1129–1157.
998 [44] Combescure A, Gravouil A. A time-space multi-scale algorithm for transient structural
999 nonlinear problems. Méc Ind 2001; 2(1):43–55
1000 [45] H.P. Wan, Y.Q. Ni, An efficient approach for dynamic global sensitivity analysis of
1001 stochastic train-track-bridge system, Mech. Syst. Signal Process., 117 (2019), 843-861.
1002 [46] G Wendt, P Erbts, A Düster. Partitioned coupling strategies for multi-physically coupled
1003 radiative heat transfer problems. J. Comput. Phys. 300(2015)327–351.
1004 [47] B Philip, MA.Berrill, S Allu, SP.Hamilton, RS.Sampath, KT.Clarno, GA.Dilts. A parallel
1005 multi-domain solution methodology applied to nonlinear thermal transport problems in
1006 nuclear fuel pins.J. Comput. Phys. 286(2015)143–171.
1007 [48] S. Krenk, Extended state-space time integration with high-frequency energy dissipation,
1008 Int. J. Numer. Methods Engrg. 73 (2008) 1767–1787.
1009 [49] Brun M, BattiA, Limam A, Combescure A. Implicit/explicit multi-time step co-
1010 computations for predicting reinforced concrete structure response under earthquake
1011 loading. Soil Dyn Earthq Eng 2012; 33(1):19–37
1012 [50] Karimi S., Nakshatrala. K B. On multi-time-step monolithic coupling algorithms for
1013 elastodynamics. J. Comput. Phys. 2014; 273: 671-705
1014 [51] Chantrait T,Rannou J, Gravouil A. Lowintrusive coupling of implicit and explicit time
1015 integration schemes for structural dynamics: Application to low energy impacts on
1016 composite structures. Finite Elem Anal Des 2014; 86:23–33

[52] Combescure A, Gravouil A, Herry B. An algorithm to solve transient structural non-linear problems for non-matching timespace domains. Comput Struct 2003; 81(12):1211–1222

[53] Faucher V, Combescure A. A time and space mortar method for coupling linear modal subdomains and non-linear subdomains in explicit structural dynamics. Comput Methods Appl Mech Eng 2003; 192(5):509–533

[54] Gravouil A, Combescure A. Multi-time-step and two-scale domain decomposition method for non-linear structural dynamics. Int J Numer Methods Eng 2003; 58(10):1545–1569

[55] B. Herry, L. Di Valentin, A. Combescure, An approach to the connection between subdomains with non-matching meshes for transient mechanical analysis, Int. J. Numer. Methods Engrg. 55 (2002) 973–1003.

[56] A. Prakash. Multi time step domain decomposition and coupling methods for non-linear structural dynamics. Ph.D. thesis, University of Illinois at Urbana-Champaign (2007)

[57] Fatima-Ezzahra Fekak, Michael Brun, Anthony Gravouil, Bruno Depale. A new heterogeneous asynchronous explicit–implicit time integrator for nonsmooth dynamics. Comput Mech 2017; 60:1–21

[58] Michal Beneš, Karel Matouš. Asynchronous multi-domain variational integrators for nonlinear hyperelastic solids. Computer Methods in Applied Mechanics and Engineering 199 (2010) 1992–2013.

[59] S. Krenk. Energy conservation in Newmark based time integration algorithms. Comput. Methods Appl. Mech. Engrg. 195 (2006) 6110–6124

[60] Gravouil A, Combescure A. Multi-time-step explicit-implicit method for non-linear structural dynamics. Int J Numer Methods Eng 2001; 50:199–225

[61] F.Menga, J.W.Banks, W.D.Henshawb, D.W.Schwendemanb. A stable and accurate partitioned algorithm for conjugate heat transfer. J. Comput. Phys. 344(2017)51–85.

[62] M. Hasan Jamal, Prakash A, Milind Kulkarni. Exploiting semantics of temporal multi-scale methods to optimize multi-level mesh partitioning. Int. J. Numer. Meth. Engng 2017; **112**:58–85

[63] Li Z, Saad Y, Sosonkina M. pARMS: a parallel version of the algebraic recursive multilevel solver. Numerical Linear Algebra with Applications 2003; **10**:485–509.

[64] Yu KP. A new family of generalized-α time integration algorithms without overshoot for structural dynamics [J] Earthquake Engng Struct. Dyn. 2008; **37**:1389-1409

[65] J. Chung, G. Hulbert, A time integration algorithm for structural dynamics with improved numerical dissipation: the generalized-α method, J. Appl. Mech. 60 (1993) 371–375.